FRICTION STIR SPOT WELDING PROCESS: EXPERIMENTAL INVESTIGATION AND NUMERICAL MODELING

BY

AHMED KAMAL MAHGOUB

A Thesis Presented to the
DEANSHIP OF GRADUATE STUDIES

KING FAHD UNIVERSITY OF PETROLEUM & MINERALS

DHAHRAN, SAUDI ARABIA

In Partial Fulfillment of the
Requirements for the Degree of

MASTER OF SCIENCE

In

MECHANICAL ENGINEERING

MAY 2015

KING FAHD UNIVERSITY OF PETROLEUM & MINERALS

DHAHRAN- 31261, SAUDI ARABIA

DEANSHIP OF GRADUATE STUDIES

This thesis, written by **Ahmed Kamal Mahgoub** under the direction of his thesis advisor and approved by his thesis committee, has been presented and accepted by the Dean of Graduate Studies, in partial fulfillment of the requirements for the degree **MASTER OF SCIENCE IN MECHANICAL ENGINEERING.**

Dr. Abdelaziz Bazoune
(Advisor)

Dr. Zuhair M. Gasem
Department Chairman

Dr. Abdel Rahman Nasr Shuaib
(Member)

Dr. Salam A. Zummo
Dean of Graduate Studies

Dr. Neçar Merah
(Member)

1/7/15
Date

Dedicated to my kind mother, dearest father, sisters and my lovely brother.

ACKNOWLEDGMENTS

First and foremost, I thank Allah the most compassionate the most merciful for giving me health, patience, and strength to complete my thesis work.

I acknowledge King Fahd University of Petroleum & Minerals for offering me the scholarship to pursue my graduate studies. I would like also to acknowledge King Abdulaziz City for Science and Technology (KACST) for funding my project.

I would like to thank all those who supported me during my work. Many thanks to my advisor Dr. Abelaziz Bazoune for supporting me throughout my study. I would like to extend my thanks to my committee member Professor Abdel Rahman Shuaib, for his precious suggestions and inputs. I also express gratitude to my committee member Professor Neçar Merah for his valuable input and assistance in this study.

Special thanks to Dr. Fadi Al-Badour for helping and assistance throughout my work. This acknowledgement is incomplete without mentioning all technical staff in the Mechanical Engineering department workshop and lab engineers in materials science lab.

Most importantly, I want to deeply thank my parents, for continuous support, love and prayers they are giving me, I would like to thank my sisters and brother for being my constant source of encouragement and strength.

TABLE OF CONTENTS

LIST OF TABLES

LIST OF FIGURES

LIST OF ABBREVIATIONS

FSSW	Friction Stir Spot Welding
FSW	Friction Stir Welding
RFSSW	Refilled Friction Stir Spot Welding
FSFSW	Flat Spot Friction Stir Welding
RSW	Resistance Spot Welding
SEM	Scanning Electron Microscope
SZ	Stir Zone
TMAZ	Thermo-Mechanically Affected Zone
HAZ	Heat Affected Zone
BM	Base Metal
FE	Finite Element
CEL	Coupled Eulerian Lagrangian
ALE	Arbitrary Lagrangian Eulerian
FEM	Finite Element Model
ANOVA	Analysis of Variance
F1	Tensile Shear Strength

N	Rotational Speed
V	Plunging Rate
DT	Dwell Time
u_i	Plastic flow velocity in x, y, z.
x_i	x,y,z directions
p	Pressure
μ	Kinematic viscosity
v	Velocity
T	Temperature
t	Time
ρ	Density of the work-piece.
dT	Change in temperature
c_p	Specific heat capacity
k	Thermal conductivity
q	Heat generated from friction deformation

ABSTRACT

Full Name : Ahmed Kamal Mahgoub Ali

Thesis Title : Friction Stir Spot Welding: Experimental Investigation and Numerical modeling

Major Field : Mechanical Engineering

Date of Degree : May 2015

The aim of the current study is to develop a friction stir spot welding process to join a pure Copper lap joint and to study the effect of key welding parameters namely, rotational speed, plunging rate, dwell time and pin tool geometry on weld strength and quality. The weld quality parameters that have been analyzed in this study are hook formation, effective upper sheet thickness, bonded region area and fracture mode.

A sound weld quality free of voids and cracks having a weld strength of 7.1 kN was obtained at 900 rpm rotational speed, 20 mm/min plunging rate and 2 seconds dwell time using a threaded tool steel pin tool. However, these welds failed in plug failure mode which is a ductile failure mode.

A finite element model was developed to investigate the effects of process parameters (rotational speed, plunging rate and dwell time) on the work-piece temperature distribution during a friction stir spot welding process. Finite element model validation showed a good agreement between measured and predicted temperatures. The maximum error was approximately 16%. According analysis of the validated finite element model results, rotational speed has the most significant effect on the peak temperature of the work-piece. On the other hand, plunging rate and dwell time have a less effect on work-piece peak temperature.

ملخص الرسالة

الاسم الكامل: أحمد كمال محجوب علي

عنوان الرسالة: لحام النقطة الإحتكاكي التحريكي: دراسة عملية ونمذجة عددية

التخصص: هندسة ميكانيكية

تاريخ الدرجة العلمية: شعبان 1436

في هذه الدراسة تم تطوير عملية لحام نقطي تحريكي إحتكاكي لوصلة نحاس متراكبة ومن ثم تم دراسة تأثير متغيرات اللحام وهي سرعة دوران الأداة، المعدل الزمني لإدخال الأداة ، زمن التحريك وشكل الأداة على القوة اللازمة لقص اللحام بالشد. تم تحليل جودة اللحام بإعتبار شكل الخطاف، سمك الطبقة العليا الفعّال، مساحة المنطقة المرتبطة ونمط فشل اللحام.

تم الحصول على وصلة لحام ناجحة خالية من الفراغات والشقوق بقوة لحام بلغت 7,1 كيلو نيوتن عند سرعة دوران أداة بلغت 900 لفة في الدقيقة، عندما كان المعدل الزمني لإدخال الأداة 20 ملمتر في الدقيقة وزمن تحريكي بلغ ثانيتين بإستخدام أداة اللحام ذات اللولب المصنوعة من فولاذ الأدوات. علاوة على ذلك فإن نمط فشل تلك الوصلة هو إنفصال الطبقة السفلى وهو نمط فشل مطيلي.

بالإضافة إلى ذلك تم تطوير نموذج عددي لمحاكاة عملية اللحام النقطي التحريكي الإحتكاكي وذلك لدراسة أثر متغيرات اللحام على توزيع درجات الحرارة. تم التحقق من درجات الحرارة المتوقعة من النموذج العددي بمقارنتها مع درجات الحرارة المسجلة مخبرياً، وُجد توافق بين درجات الحرارة في النموذج مع درجات الحرارة المسجلة مخبريا بنسبة خطأ قصوى بلغت 16%. بالإضافة إلى ذلك وجد أن سرعة دوران الأداة ذات أعلى تأثير على درجة حرارة المادة الملحومة القصوى، بينما وُجد أن المعدل الزمني لإدخال الأداة و زمن التحريك لهما تأثير أقل على درجة حرارة المادة الملحومة القصوى.

Chapter 1

Introduction

1.1 Friction Stir Spot Welding Process

Friction Stir Spot welding (FSSW) is a suitable process for welding materials that are difficult to weld using fusion welding. This process is considered as a derivative of Friction Stir Welding (FSW) technique that was invented in 1991 by TWI in UK and was initially applied for joining Aluminum alloys. With time, the process found many applications and spread to include more similar and dissimilar materials, such as steel, Magnesium and polymers. In 2000, Kawasaki company invented and patented Friction Stir Spot Welding process as alternative to resistance spot welding in automobiles industry [1].

Many studies reported that the process can meet some challenges of rapid improvement in automobiles manufacturing [2]. It can replace fusion welding in electric resistance welding and non-permanent rivets joints because it is a solid-state and environmentally friendly process. In FSSW process, a rotating tool penetrates a lap joint to a predetermined depth and dwell time to join two materials taking the stirring only (only rotating inside the material) before retreating and exit leaving a solid-state joint. The joint is produced as a result of mixing a softened material around the shoulder and pin caused by frictional heat developed during plunging and stirring phase. Figure 1.1 shows friction stir spot welding phases.

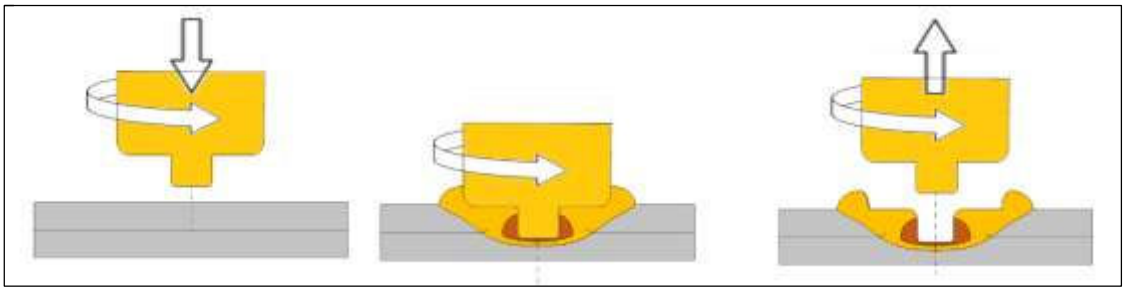

(a) (b) (c)

Figure 1.1: Friction Stir Spot Welding Phases, (a) Plunging Phase, (b) Stirring Phase, (c) Retracting or Drawing out Phase

1.2 Copper and Copper Alloys Current Welding Processes

According to Mishra *et al.* [3] high pure Copper thermal diffusivity made welding of it a real challenge due to high heat dissipation during the process. High heat dissipation prevents localized melting and obtaining a successful joint. Soldering and brazing are the most important welding processes for Copper but they do not make strong or load carrying joints.

1.3 Industrial Applications

Copper has many electrical and heat transfer applications. One of pure Copper uses is the busbars, which are strips or bars of Copper, brass or Aluminum that conducts electricity within an electrical apparatus such as switchboard, distribution board, substation, battery bank and others. The main purpose of these busbars is to conduct a substantial current of electricity.

Busbars are connected to each other by bolting, clamping, or welding. Often, joints between high-current bus sections have precisely-machined matching surfaces that are silver-plated to reduce the contact resistance. FSSW can be an attractive alternative to

join these busbars to each other providing a perfect connection that can reduce power losses in these connections. Figure 1.2 shows busbars in an electric distribution board.

Other applications of pure Copper can be found in trucks, radiators, heat sinks and air conditioning.

Figure 1.2: Busbars in Electrical Distribution Boards, [4]**.**

1.4 Advantages of Friction Stir Spot Welding

FSSW has similar advantages to those of FSW as reported by Mishra *et al.* [3]. Choi *et al.* [5] compared resistance spot welding (RSW) and FSSW. They showed that FSSW offered 90% energy saving and 40% equipment saving due to its minimal equipment requirement.

1.5 Friction Stir Spot Welding Process Metallurgy

In friction stir spot welding, the bonding conditions between the upper and lower sheet can be classified into three bonding regions, these regions are complete bonded region, partial or transition bonded region and mechanical bonded region.

- **Complete Bonded Region**

In this region, the interface between welded plates cannot be identified and full bond is formed. Figure 1.3 shows FSSW metallurgical bonded regions. Bonded region term will be used for referring to complete bonding region throughout this study for simplicity. Yuan *et al.* [2] reported that the complete bonded region area is the load carrying area.

- **Partial Bonded Region**

The partial bonded region is a transition region between full metallurgical bond and mechanically bonded region. It is also called the hook. In this region, metallurgical bond starts to form, the interface can be easily identified.

- **Mechanical Bonded Region**

This region is also called kissing bond. Only mechanical contact is present between upper and lower sheets in this region.

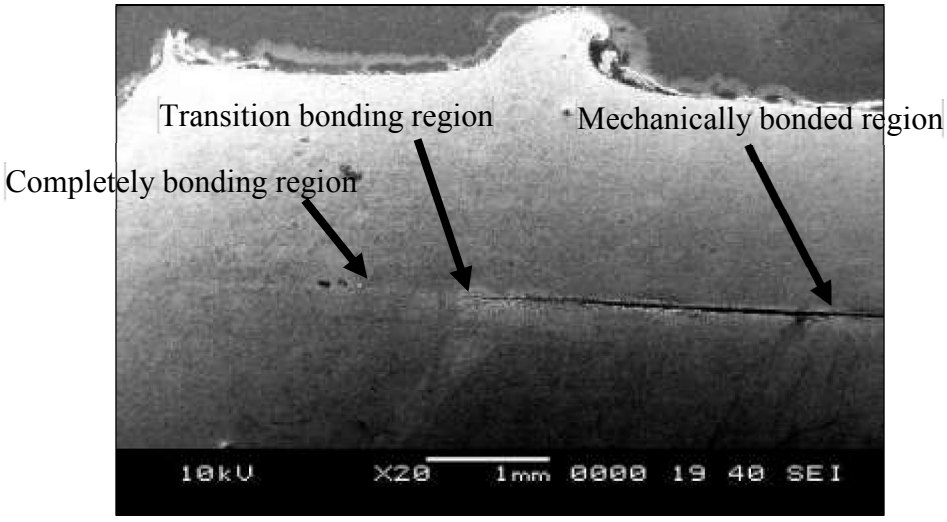

Figure 1.3: SEM Macrograph for FSSW Metallurgical Bonding Regions

1.6 Research Objective

The high thermal conductivity in pure Copper presents a real challenge in welding of such materials using resistance spot welding because of the high heat input required to the weld. FSSW may be considered as an attractive alternative to weld such materials.

The main objective of the present work is to develop FSSW process for joining a pure Copper lap joint, to study the effect of key welding parameters on weld strength and quality and to find the best set of welding parameters, which result in sound weld quality.

The specific objectives are:

- to investigate the effect of welding parameters, namely, rotational speed, plunging rate, dwell time and pin tool geometry on friction stir spot welds strength.
- to evaluate the effect of welding parameters on weldment quality. For weldment quality analysis hook formation, effective upper sheet thickness and complete bonded region area are considered.
- to analyze the effect of those welding parameters on fracture mode.
- to develop FE model to study the effect of welding parameters on temperature distribution and plastic strains developed during the welding process.

1.7 Motivation of the Study

To the knowledge of the author, so far no work has been reported in FSSW of pure Copper. This motivated the author to carry out a comprehensive investigation aimed to analyze the effect of welding parameters on pure Copper weld joint and to obtain full understanding of the process.

1.8 Thesis Structure

This thesis includes six chapters. The arrangement of these chapters will be as follows:

Chapter one is an introduction that includes general background of the process, metallurgy of the process, objective and work justification.

Chapter Two is a literature review about the subject undertaken and it highlights the most important finding obtained in published work.

Chapter Three presents experimental work methodology and experimental work matrices.

Chapter Four presents experimental work together with discussion and interpretation of the results.

In **Chapter Five** a finite element model technique, using Abaqus® Explicit solver is adopted for the analysis. Boundary conditions, materials modeling, as well as interaction modeling are presented. Validation of the model is carried out. Temperature distribution, in the weld cross-section is presented for different boundary conditions (welding conditions).

Chapter Six presents conclusion and future refinement of the present work.

Chapter 2

LITERATURE REVIEW

Previous published work on experimental studies, numerical modeling of FSSW will be briefly reviewed in this chapter. This chapter also presents investigation of FSW of pure Copper since there are thermomechanical similarities between FSW and FSSW of pure copper.

2.1 Experimental Studies in Friction Stir Spot Welding

Since its invention, researchers are trying to understand FSSW process [6,7], that lead to optimizing the process parameters (plunging rate, plunging depth, rotational speed, dwell time, retracting rate, tool geometrical parameters) in order to obtain sound weld. Other researchers are focusing in studying material flow in FSSW process [8]. Most of these studies focused on Aluminum and Aluminum alloys [8], polymers [9] and few other materials such as Magnesium [6,10] as application for the process.

Effect of welding parameters on the weld tensile shear strength has been studied in the past by several investigators as reported by Hirasawa *et al.* [8]. Yuan *et al*. [6] studied the effect of tool pin profile on joint strength in FSSW of Aluminum alloy 6016. They used one conventional tool with a step spiral pin. The other one having three off-center (OC) hemispherical pin features. The OC gave higher lap shear strength. These authors reported that the shoulder penetration depth of 0.2 mm and tool rotational speed of 1500 rpm for conventional pin and 2500 rpm for OC pin tool have an optimum value at which the weld strength reaches the maximum value of 3.3 kN. Badarinarayan *et al.* [11]

compared the weld strength and hook formation (partial metallurgical bonding) between cylindrical pin tool and triangular pin tool with concave shoulder in welding of 5754-O sheets. The investigation showed that using triangular pin resulted in a wider bonding region and a weld strength that is twice larger than the one achieved using cylindrical pin tool. They also studied hook formation and weld strength of 5754-O sheets. Moreover, they studied the effect of shoulder type on static weld strength. The concave shoulder resulted in the highest static strength of 3.5 kN compared to flat and convex shoulder type.

Shin *et al.* [9] performed an experimental study for dissimilar welding of bulk metallic glass (BMG) alloy to lightweight crystalline alloys. They studied the influence of tool geometry with round and triangular shaped pins on FSSW performance. They found that the triangular pin tool produced more chips. Its cutting effect resulted in lowering the tool axial load. The workpiece temperature in the early stage of the process as compared to the round pin case failed in a lower failure load compared to round pin tool.

Merzoug *et al.* [12] studied the effect of tool rotational speed, and plunging feed on FSSW of 6060 Aluminum alloy. They reported that the temperature needed to produce enough plastic effect in metal and achieve the best weld reached about 80% of melting temperature.

A limited published work on comparison of FSSW and RSW can be found in litreature [13,14]. Kulekci *et al.* [13] performed a comparative analysis in terms of hardness distribution and tensile shear strength between resistance spot welding (RSW) and FSSW for the material EN AW 5005 Aluminum alloy. They obtained a weld strength that is more than 250% higher than that obtained by RSW. It was also found that the

tensile shear strength increases with the increase of pin height while it decreases with the increase of welding time. Another comparative study between FSSW and RSW was performed by Khan *et al.* [14] in welding of dual phase steel DP600. The micro-hardness distribution in stir zone of FSSW was 25% higher compared to RSW. Comparison of surface finish showed that better surface finish resulted when using RSW process. Better surface finish is preferred in automobile industry, [14]. Keyhole and oxidization resulted in poor FSSW weld surface finish, which can be minimized by using inert gases.

Yang *et al.* [15] investigated the material flow in FSSW of Magnesium AZ31 using Cu foil as a tracer in different configurations (between upper and lower sheet, at the top of the upper sheet). According to the authors, putting Cu foil in the sheets interface can give an idea about material flow within the process. The Cu foil flows with the parent metal while it affects the material flow. Yang *et al.* [15] pointed out that the threaded pin tool produced intermixed stir zone. On the other hand, smooth plain cylindrical pin tool failed to produce intermixed stir zone.

Su *et al.* [16] investigated the intermixing in FSSW of dissimilar AA5XXX to AA6XXX. The authors have noticed the absence of intermixing when using simple pin tool. Intermixing was observed when using threaded pin tool with dwell time. This resulted in enhanced material flow.

Sun *et al*. [17] studied frequency induction preheating in FSSW of low carbon steel. They observed slight increase in stir zone grain size for the preheated welds compared to conventional welds. This resulted in an increase in the tensile strength by approximately 50% for preheated joint compared to conventional process.

2.2 Numerical Studies in Friction Stir Spot Welding

Numerical modeling of FSSW process is receiving a great deal of attention by many researchers [8, 18, 19, 20, 21], and the number is increasing rapidly. Mandal *et al.* [18] developed thermo-mechanical model using Abaqus® to simulate plunging step in FSSW of Aluminum 2024. The authors compared the attained temperature distribution with experimental measurements from literature. A maximum error of about 20% was obtained. The axial force was approximately 4 times larger than experimental measurements.

Assidi *et al.* [19] developed an Arbitrary Lagrangian Eulerian (ALE) finite element model using Forge3® finite element software. The aim of their work was to find a numerical approach for accurately computing the interaction between tool and plate by computing the frictional contact surface. They used Norton's friction model. It was observed that welding forces and tool temperatures is very sensitive to friction coefficient. Their predicted welding force did not match well with experimental measurements for low coefficient of friction and welding speed.

Reilly [20] developed a FE model to model the thermal aspect of the process to include deformation behavior without the need for a fully-coupled approach in pinless FSSW of Aluminum to Aluminum and Aluminum to steel welds. He used sequential small-strain analysis method. However, the author didn't show any validation with experiment for his model.

Awang [21] studied the friction phenomenon and heat generation during FSSW process. Arbitrary Lagrangian Eulerian (ALE) finite element model was developed using Abaqus/Explicit. He defined the friction coefficient at the interface between the workpiece and the welding tool as dependent on temperature, pressure and slip rate with sliding

Coulomb friction. Close results were obtained with those obtained by Su *et al.* [22] for only 1.5 seconds. The authors attributed this discrepancy to the ALE model time consuming and needs large storing memory.

Modeling of the material flow during the welding process took also its share in developing FEM in literature. Hirasawa *et al.* [8] studied numerically the effect of pin tool geometry on temperature distribution and the plastic flow of material during FSSW process. The plastic flow was analyzed with the elastic–plastic deformation model using the particle method. The study concluded that the triangular pin tool, due to its inherent geometry, showed enhanced material flow leading to high weld strength.

Grujicic *et al.* [23] investigated the material flow in friction stir welding process using combined Lagrangain Eulerian domain, the workpiece material is treated as an Eulerian component while FSW tool is treated as a Lagrangian component. Temperature dependent material properties and Johnson-Cook model were used to model the material flow. Grujicic *et al.* [23] reported that Combined Lagrangian Eulerian method is efficient in terms of modeling the material flow during the process.

2.3 Keyhole Remedies Literature

The most critical drawback in FSSW is the keyhole that is left in the workpiece after retracting the pin tool during the retraction phase. This hole weakens the weld joint. Recently some studies proposed several methods to alleviate and remove the keyhole problem [25,26]. One of these solutions is to use pin less tool for flattening and closing of the keyhole in a process that is called refilled friction stir spot welding. Venukumar *et al.* [25] compared FSSW with refilled FSSW (RFSSW) using friction forming process. In this

process, an additional tool called friction forming tool used to retain the extruded material after drawing out phase. Analysis of shear strength showed that refilled friction stir spot welding (RFSSW) process provided a higher strength compared to conventional FSSW. Moreover, the strength of the conventional FSSW weld was decreasing by increasing the rotational speed, while the strength of RFSSW was increasing by increasing the rotational speed (only 7% higher strength at 900 rpm and almost double the strength at 1800 rpm).

Sun *et al.* [26] used Flat Spot Friction Stir Welding (FSFSW) technique to weld 1.0 mm Aluminum sheet thickness to mild steel sheet. The FSFSW is a modified process of FSSW that aims to alleviate the keyhole problem in FSSW. It consists of two steps, the first one is a plunging step above a round dent made on the back plate. After that a probe-less rotating tool is used to flatten the weld surface. The authors concluded that sound Al/Fe welds with similar microstructure and mechanical properties can be obtained after flattening step.

Muci-Küchler *et al.* [27] modeled the process of modified refilled FSSW using a coupled thermo-mechanical finite element model. The authors studied plunging phase in this investigation. Clamps were included in the model to squeeze the extruded material during plunging, which helps in using this squeezed material to refill the keyhole in refilling step.

Zhang *et al.* [28] used a retractable pin tool to join 3.0 mm thick Magnesium alloy sheet to 1.0 mm galvanized mild Steel. In this attempt, the effect of stacking sequence of Magnesium and mild Steel, rotational speed, plunge depth and pin tool diameter were investigated. They studied the effect of rotational speed between 1200-1400 rpm and concluded that using of 1200 rpm rotational speed resulted in insufficient heat generation.

According to the authors stacking sequence is a critical variable that would affect the weld formation. The authors found that when the Magnesium sheet was placed on the top of mild steel, the frictional heat produced during the process dissipates to the Magnesium instead of steel. This resulted in a poor quality weld.

Tozaki *et al.* [29] and Cox *et al.* [30] used a scrolled type shoulder without probe in FSSW of Aluminum alloy and found that shoulder plunge depth has a significant effect in FSSW process. Tozaki *et al.* [29] showed that the scroll shoulder has a superior performance in terms of weld quality compared to conventional shoulder in welding of 6061-T4 sheets. Cox *et al.* [30] reported that rotational speed and dwell time have a controlling effect on probe-less friction stir spot welding process. In addition, they found that stronger weld was obtained when low rotational speed and dwell time were used.

Shen et al. [31] analyzed modes of failure in refill friction stir spot welding of Aluminum 7075-T6. According to the authors, precipitation state has a dominant effect on grain size at different weld regions. Three types of failures were pointed out by Shen et al. [31], namely, nugget debonding, plug of top sheet and plug of bottom sheet.

2.4 Formation of Voids and Localized Melting in FSSW Literature Search

Some investigations in literature highlighted the formation of voids, effect of localized melting on tool slippage in FSSW [32]. Gerlich et al. [32] analyzed strain rate and temperature variation in stir zone of Al 7075-T6 spot welds. They found that the strain rate decreases from 650 to about 20 s-1 when the tool rotational speed increased from 1000 to 3000 rpm. This happened because tool slippage occurs when the welding parameter settings facilitate transient local melting due to high heating rate at high rotational speed.

In this study, the authors employed Zener–Hollomon relation to find the strain rate. Transmission Electron Microscopy (TEM), and Electron Back Scatter diffraction (EBSD) characterization techniques were used to find microstructure sub-grain size, thermocouples also used to measure the temperature during the process. On the other hand, Reily [20] employed Zener-Hollomon relation for strain rate calculation. They found the effect of rotational speed on strain rate. Transmission Electron Microscopy (TEM) and Electron Back Scatter Diffraction (EBSD) were used for sub grain size calculation. Reily [20] pointed out that Zener-Hollomon relation can't give accurate results when there is a phase change experienced at high heating rate (high rotational speed).

Gerlich *et al.* [7] found evidences of local melting in AA7075 alloy by quenching high plunging rate friction stir spot welds. In this study, the authors compared strain rate measurement using Zener–Hollomon relation for AA2024 to AA7075 and AA5754 to Al6061. They concluded that the material being welded and rotational speed parameters have a significant effect on the average strain rate.

Wang *et al.* [33] studied microstructure and failure mechanism in Al6061 during lap shear test. They compared macrographs before the specimen failed, at different loading steps during specimen failure. They found that the shear initiates from the nugget circumferential region between Heat Affected Zone (HAZ) and Thermo-Mechanically Affected Zone (TMAZ), then propagates through weld thickness.

Fatigue analysis of FSSW was also carried out as found in some investigations in literature [34]. Wang *et al.* [34] investigated fatigue in FSSW for Aluminum 6061 T6 experimentally. Close results were attained compared to Paris fatigue model. They stated that fatigue cracks in FSSW grow along the circumference of the weld nugget, then

propagate through the sheet thickness, before fracture of the specimen occurs. The authors described the bonding in spot welded joints by reporting that the interfacial surfaces become a zigzag line before it disappears in stir zone where full bonding is happening. Closer view to zigzag formation showed that it's a strip of voids formed due to high pressure and plastic deformation. They also performed fatigue test at different cycling loads and found that the joint behaved in a similar manner.

Friction stir spot and the refilled process were studied in terms of fatigue response by Uematsu *et al.* [35] who studied the response of refilled FSSW with the weld without refilling in Al–Mg–Si alloys. They performed tensile shear tests and fatigue fracture tests on both welds. Refilled welds showed better tensile strength. Both welds failed by shear type fracture through the nugget. Fatigue strength was almost the same for both welds.

Mitlin et al. [36] studied the effect of different tool penetration depth on the microstructure and size of each metallurgical region beneath the shoulder in welding of Al-6111. They found evidences of voids formation in the material.

2.5 Friction Stir Welding of Copper

Copper is difficult to weld using conventional welding techniques because it has high thermal conductivity. The general trend encountered in the published work in FSW of pure copper is to understand the effect of welding parameters on weld quality. Some other works were devoted to study the effect of tool geometry on microstructure, surface morphology and micro-hardness profile of resulted joint. Kumar *et al.* [37] investigated the effect of pin tool geometry on surface morphology and ultimate tensile strength. Tapered cylindrical, triangular, square pentagonal, and hexagonal pin tools were studied. Analysis

of surface morphology showed that the lowest amount of flash was observed in the square pin tool welds, which experienced superior ultimate tensile strength and very fine microstructure of the weld zone. The authors concluded that the pin tool geometry has a significant effect on the mechanical properties of the joints. Welding efficiency of 85% was obtained for square pin tool. Park *et al.* [38] analyzed the effect of rotational speed and welding speed on stir zone microstructure and tensile strength of the weld for 60% Cu–40% Zn copper alloy. They found that the stir zone grain size is decreasing with decreasing of the heat input, and the welding speed has no significant effect on the tensile strength.

Sakthivel and Mukhopadhyay [39] used hardened simple cylindrical pin tool having a hardness of 55 HRC to make a butt joint of 2 mm thick pure copper plates. Welding efficiency of 85% with defect free weld was obtained at tool rotational speed of 1000 rpm and welding speed of 30 mm/min. Furthermore, the welds microstructure was analyzed in this study. Elongated grains were observed in TMAZ. Coarse grains were observed in HAZ with the lowest hardness and fine equiaxed grains in weld nugget, which has higher hardness with respect to the base metal. Meran *et al.* [40] correlated the axial tool force to the weld quality. The study showed the importance of having constant axial tool force to obtain a good appearance and strong joint.

Cederqvist *et al.* [41] derived a relationship between power input and tool temperature to control the stability of the process and to keep the tool temperature within a low temperature range. The authors reported that the risk of probe fracture increases with tool temperature. Andersson *et al.* [42, 43] reported that high temperature tool steel pin tool is

not suitable in friction stir welding of 10 mm thick pure copper sheet due to softening of the pin tool at tool temperature of 540ºC.

Galvão *et al.* [44] studied the effect of three shoulder geometries in FSW of copper thin sheets. Internal defect was observed for all geometries under study, namely, flat, conical and scrolled type at low rotational speed. Using of scrolled type shoulder resulted in finest grain regardless of spindle rotational speed. In terms of material flow, the authors reported that the scrolled type shoulder developed adequate material flow around the pin and the highest heat input to the weld.

Heidarzadeh *at al.* [45] also carried out experimental investigation of FSW of pure copper using response surface methodology design of experiment. They concluded that increase of heat input increases elongations percent. They also observed more dimples in tensile test fractographs at high heat input indicating ductile fracture mode.

2.6 Pin Tools Materials in FSW of Pure Copper

Table 2.1 summarizes some pin tool materials used in literature for friction stir welding of pure copper or copper alloys.

2.7 Pin Tool Materials Literature Search

Table 2.2 summarizes the operating conditions for FSSW and corresponding work-piece and pin tools materials.

Table 2.1 Pin Tool Materials and Welding Parameters for Welding of Copper and Copper Alloys

#	Author	Pin Tool Material Used	Rotational Speed [rpm]	Remarks
1	Kumar *et al.* [37]	H13 Tool steel	900	-
2	Park *et al.* [38]	Not mentioned	1000-1500	- Dissimilar Cu/Brass FSW. - 12-4-2 (shoulder diameter, probe diameter, and probe length, respectively).
3	Sakthivel and Mukhopadhyay [39]	Oil Hardned steel	1000	Material not specified
4	Cederqvist *et al.* [41]	Not mentioned	400-450	- Probe fracture due to high tool temperature (above 950^{o}C) was experience and mentioned in this study. - The authors also mentioned that very low rotational speed may damage the machine.
5	Heideman *et al.* [46]	H13 Tool steel	2000	- Al/Cu FSW - 2000 rpm May not be suitable for Cu-Cu welding because Al/Cu is colder
6	Lee *et al.* [47]	Tool steel	1250	Material not specified
7	Xu *et al.* [48]	Not mentioned	400-800	According to the authors almost 100% weld efficiency was achieved at 400 rpm.

Table 2.2 Pin Tool Materials, Work-Piece Material and Welding Parameters

#	Author	Workpiece material	Pin Tool Material	Pin tool Feature (Shoulder Diameter-Pin Diameter) [mm]	Rotational speed range [rpm]	Plunging Rate range [mm/min]	Dwell Time Range [seconds]
1	Cox *et al.* [30]	AA2024-T3	01 AISI oil hardened tool steel	Scrolled-spherically tapered shoulder 10.2 mm	750-1750	7.8-18	2-6
2	Meran *et al.* [40]	Copper/brass	X155CrMoV12 – 1	Plain 5-12	1500		
3	Karthikeyan *et al.* [49]	AA2024	High Carbon steel	Threaded 5.4-16.2	600-1400	4-20	3-7
4	Fernandez *et al.* [50]	cast Aluminum	AISI 01	threaded 6.3	500-1000	-	-
5	Cao *et al.* [51]	AZ31B-H24 Mg alloy	H13 steel	6.35-19	500-2000	-	2.5
6	Mahgoub *et al.* [52]	Pure Copper	AISI 01 oil hardened	Plain 5-11.52	900-1200	20	2-4

Chapter 3

EXPERIMENTAL WORK

In this chapter the experimental work preparations, methodology and setup are presented. Then a design of Experiment (DoE) is carried out using Minitab® [53] to study the effect of process parameters on commercial pure copper FSSW weld quality and strength. Experimental work preparation includes pin tool design, manufacturing and heat treatment for the pin tool to meet the desired hardness value.

3.1 Chemical Composition of Pin Tools Material

The chemical compositions of pin tool material AISI 4140 and AISI-01 are shown in Table 3.1.

Table 3.1 Measured Chemical Composition for AISI 4140 and AISI 01 in percentage (%)

Material	C	Si	Mn	Cr	Cu	Ni	Mo	V	W	Fe
AISI 4140	0.511	0.214	0.763	0.924	-	0.117	0.142	-	0.0513	97.0
AISI 01	1.42	0.41	0.354	0.434	0.0282	0.0718	0.0206	0.0917	0.0427	97.1

3.2 Base Material Chemical Composition and Mechanical Properties

The work-piece material joined in this study is commercial pure copper. Elemental analysis is performed for chemical composition. Table 3.2 presents pure copper chemical composition. The percentage of pure copper in the commercial pure copper material is 98.6% while the rest is other constituents including Zinc, phosphore and Cobalt.

Table 3.2 Measured Pure Copper Chemical Composition in percentage (%)

Zn	Pb	Co	Cu
0.23	0.165	0.146	98.6

Commercial pure copper was tested to measure the mechanical properties. Samples were cut according to ASTM E8M Standard [54]. Instron 5589 tensile test machine is used in the tensile test. Table 3.3 presents pure Copper mechanical properties. The base material yield stress is 157.4 MPa.

Table 3.3 Measured Pure Copper Mechanical Properties

Material	Yield Stress [MPa]	Ultimate Tensile Stress [MPa]	Maximum Tensile Strain (%)	Density [kg/m^3]
Commercial Pure Copper	157.4	216.7	37.9	8940

3.3 Pin Tools Designs

Simple and threaded pin tools were used in the experiments of FSSW as shown in Figure 3.1. The pin tools have 5.0 mm diameter and 3.0 mm length. Threaded and simple tools have similar dimensions. The main difference is the threaded feature in the threaded pin tool.

3.4 Pin Tools Heat Treatment

Heat treatment of pin tools was carried out to obtain a hardness of 55 HRC. This hardness is appropriate for FSW of pure copper according to Sakthivel and Mukhopadhyay [39].

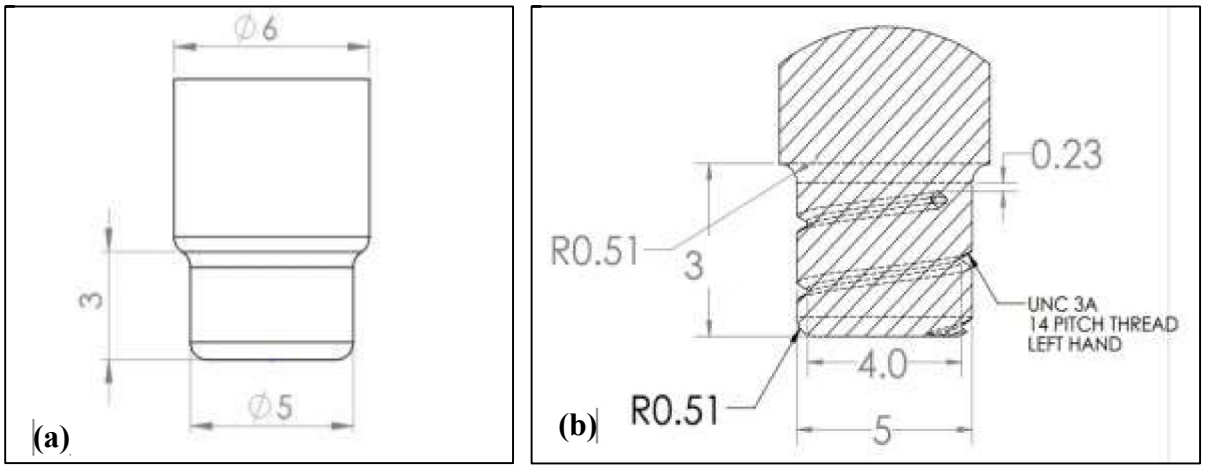

All dimensions are in mm, all fillets are 0.5 mm.

Figure 3.1: (a) Simple Pin Tool Design, (b) Threaded Pin Tool Design

To obtain accurate dimensions for the pin tools according to the design, heat treatment allowance was considered. Figure 3.2 shows the relation between tempering temperature and length change in inches for oil hardened tool steel AISI "01". This Figure was consulted to obtain the desired pin diameter and length after heat treatment. At tempering temperature of 250ºC (482 º F), the allowance is 0.0014 inch (0.035 mm). However, 0.035 mm was added to 6 mm diameter pin tool shank as heat treatment allowance, which fitted properly into tool holder. Table 3.4 illustrates heat treatment procedure.

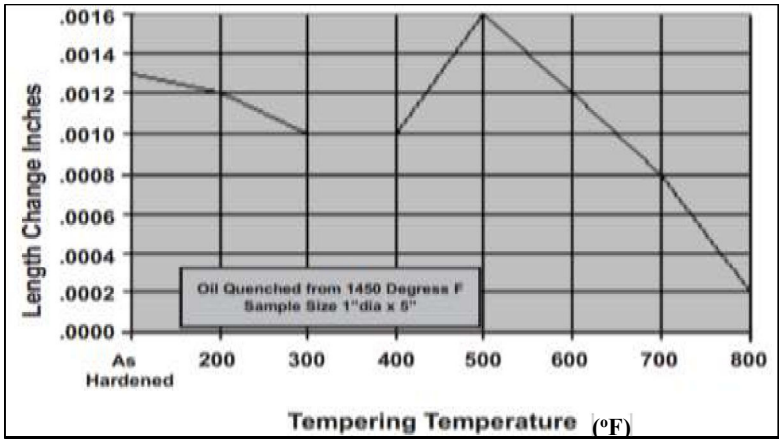

Figure 3.2: Heat Treatment Allowance for AISI 01

Table 3.4 Pin Tools Heat Treatment

Pin tool material	Hardening Temperature [ºC]	Quenching Media	Tempering Temperature [ºC]	Hardness (HRC)
AISI "01"	800	Oil	250	55
AISI 4140	850	Water	100	55

3.5 Shoulder Geometry

Figure 3.3 shows scrolled concave steel shoulder manufactured by MTI [55] is used in the experimental work. The scrolled feature on shoulder surface enhances material flow and mechanical work produced by the shoulder. The shoulder has a diameter of 11.52 mm and 6 mm internal diameter to insert the pin tool.

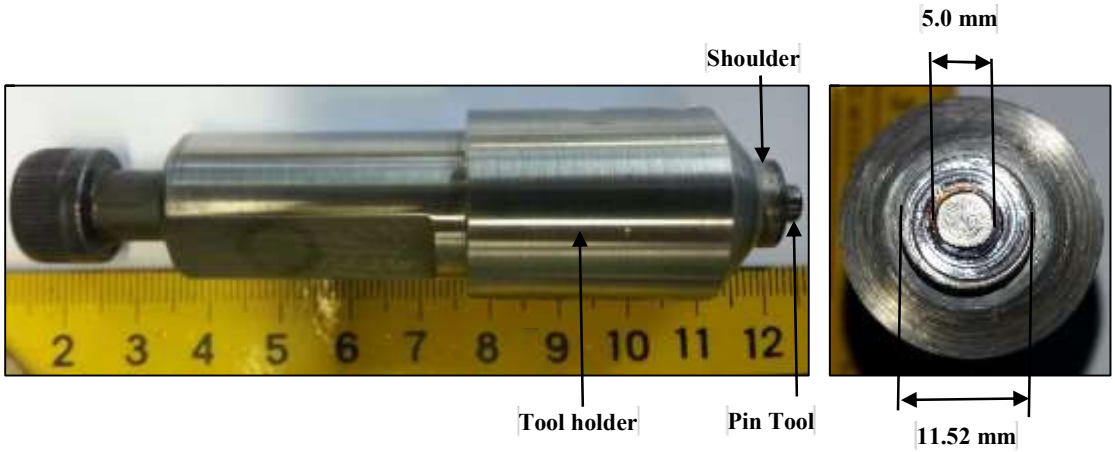

Figure 3.3: Scrolled Type Shoulder Used in Experimental Work (All Dimensions in mm)

3.6 Experimental Setup

Two copper plates, having dimensions of 138 mm length, 60 mm width and 2.0 mm thickness were selected. The gripping length is 62.5 mm, the overlapping area is 45X60 mm^2 according to American Welding Society Standard [56]. Special fixtures were designed, manufactured and used to assure the lap joint alignment, and reduce welding

setting time. Clamps with screws were also used for mounting the upper plate over the lower one. Clamps were tightened to prevent the work-piece from pulling up. A spacer was used to bear upper plate in the lap joint configuration. Figure 3.4 shows the experimental setup.

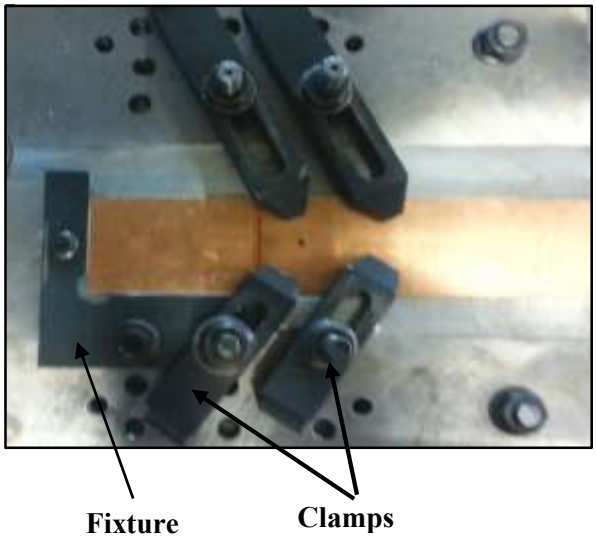

Figure 3.4: Experimental Setup Fixtures

Experimental work was performed using FSW machine MTI RM-1 FSW developed by Shuaib *et al.* [57]. This machine is fully controlled with embedded data acquisition system capable of providing all experimental measurement needed, such as spindle torque, forging force, instantaneous plunging rate and x, y, z movements and forces. Figure 3.5 shows the MTI RM-1 friction stir welding machine used in the experimental work. For tensile shear strength test coupons were prepared according to AWS/ANSI/SAE D8.9-97 standard as shown in Table 3.5 and Figure 3.6.

Figure 3.5: MTI-RM-1 FSW Machine

3.7 Experimental Work Methodology

After performing FSSW on the lap joint configuration. Mechanical and metallurgical tests have been performed to test the quality of the weldment. These tests are listed below.

3.7.1 Tensile Shear Strength Analysis

Tensile test machine Instron® 5589 is used to perform tensile shear strength tests of friction stir spot welds. Tensile tests were conducted at 1 mm/min cross head. Two spacers were glued to the lap joint to obtain a flat, aligned tensile test coupon as shown in Figure 3.6. Two samples were tested for each set of welding parameters.

Table 3.5 AWS Standard D8-9 1997 [56]. All Dimensions are in mm.

Sheet Thickness	Coupon Length	Coupon Width	Overlap Length	Sample Length	Unclamped Length	Gripped Length
0.6-1.29	105	45	35	175	95	40
1.3-3.00	138	60	45	230	105	62.5

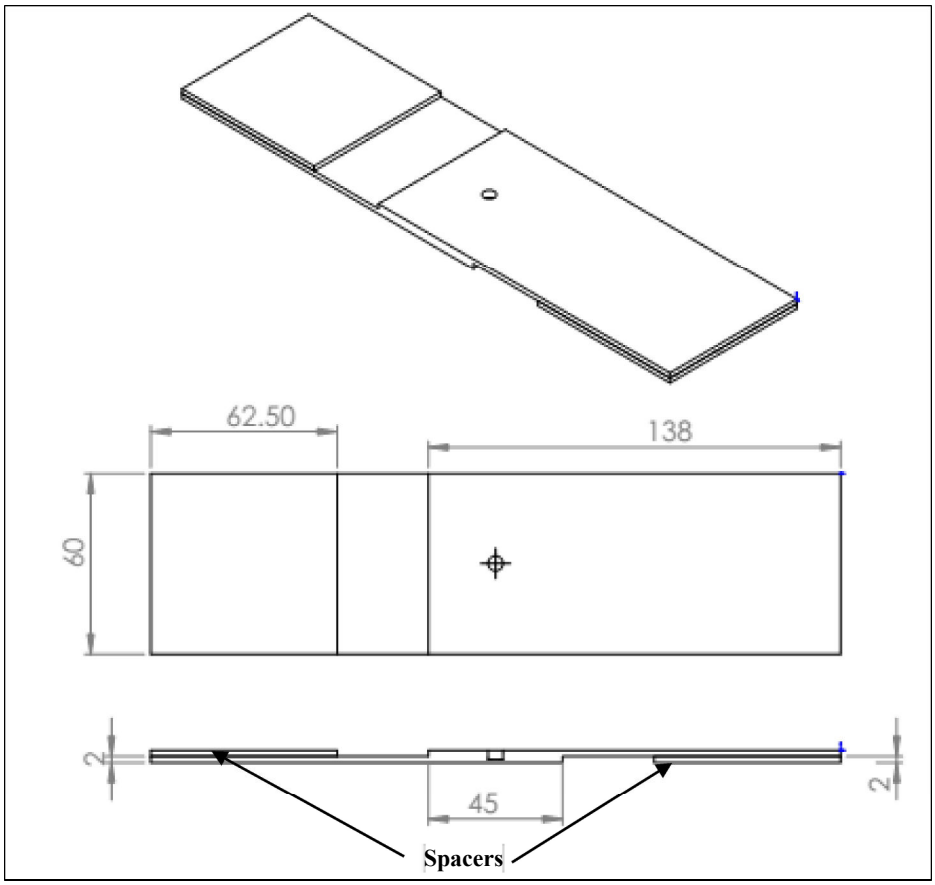

Figure 3.6: Weld Joint Dimensions

3.7.2 Evaluation of Weld Joint Quality

Weld joints characterizations were carried out to understand the effect of welding parameters on weld microstructure, macrographs, micrographs and fractographs after tensile shear failure.

The following tools were used in characterizing the weld quality:

- Optical microscope INFINITY 8.0 for microstructural analysis and grain size determination.

- The Scanning Electron Microscopy SEM analysis using JEOL Scanning Electron Microscopy is performed to obtain a high magnification images of the following regions:
    - On the hook feature to examine weld quality in terms of formation of voids and to measure effective upper sheet thickness.
    - On the fracture surfaces of the tensile test failed samples.

3.7.3 Experiment Design Matrices

The key parameters that controls FSSW process and determines welds tensile shear strength are rotational speed (N), plunging rate (V), dwell time (DT), pin tool length, and pin tool geometry. These parameters were highlighted in references [6, 8, 12, 32, 57].

The process parameters that were considered are rotational speed, plunging rate, dwell time and pin tool geometry. According to studies that have been reported in FSW of pure copper, many investigations reported that a sound weld quality was obtained at 900 rpm and 1200 rpm rotational speed [37, 47]. Kumar *et al.* [37] reported that a sound weld was obtained at 900 rpm rotational speed and 40 mm/min welding speed in FSW of pure copper. On the other hand, Lee *et al.* [47] investigated FSW of pure copper and they reported that the optimum welding condition is 1250 rpm rotational speed and 61 mm/min welding speed. Moreover, preliminary experiments in the current work revealed that the welds that were produced at 600 rpm rotational speed have relatively low weld strength compared to 900 rpm and 1200 rpm rotational speed. In this study, rotational speeds of 1200 and 900 rpm were considered.

Preliminary experiments were conducted to identify range of welding parameters as well as testing of the experimental setup, fixtures, and clamps. These experiments showed that some modifications on the setup were necessary to eliminate movement of the work-piece during welding.

Welding parameters at 1200 rpm rotational speed, 20 mm/min plunging rate, 4 seconds dwell time and AISI 01 pin tool material were selected as to deliver the highest heat input applied in the experiment matrix that was considered in this study. Table 3.6 shows the experiment work matrix.

Table 3.6 Main Factorial Design of Experiment Matrix

Experiment No.	N [rpm]	V [mm/min]	DT [seconds]
1	1100	40	3
2	1200	20	2
3	1200	20	4
4	1200	60	2
5	1200	60	4
6	900	20	2
7	900	20	4
8	900	60	2
9	900	60	4

3.7.4 Effect of Pin Tool Feature Experimental Matrix

Threaded and simple cylindrical pin tools were considered. The threaded pin tool was fractured at 1200 rpm rotational speed due to excessive heat input, so only 900 rpm rotational speed is studied for the threaded pin tool. According to full factorial design of experiment, the 60 mm/min plunging rate using simple pin tool resulted in poor weld strength and quality, for that reason only 20 mm/min plunging rate is considered for the

threaded pin tool analysis. Table 3.7 illustrates the effect of pin tool geometry experiment matrix.

Table 3.7 Effect of Pin Tool Geometry Experiment Matrix

Experiment No.	Pin Tool Feature	N [rpm]	V [mm/min]	DT [seconds]
1	Simple	900	20	2
2		900	20	4
3	Threaded	900	20	2
4		900	20	4

3.7.5 Microstructural Analysis

One sample from each set of welding parameters cited in Table 3.6 was sectioned and mounted in epoxy resins, followed by grounding, mechanically polishing and etching using a solution of 1 gram $FeCl_3$, 10 ml HCl added to 100 ml desalinated water, to reveal the welded zone micro-structure. Infinity 1 optical microscope was used to obtain microstructure of welding zones.

Chapter 4

EXPERIMENTAL WORK RESULTS

This chapter presents experimental work results that include effect of welding parameters (Rotational speed, Plunging rate, Dwell time and pin tool geometry) on the following:

- Forging force by the pin tool
- Tensile shear strength.
- FSSW weldment quality, which includes the following.
    - SEM micrographs for hook feature.
    - Effective upper sheet thickness.
    - Metallurgical bonding region Area.
    - Fracture surface morphology analysis.

4.1 Effect of Welding Parameters on Forging Force

Forging force is the pin tool reaction to plunging of the pin tool into the work-piece. Lower forging force was observed at lower plunging rate. Figure 4.1 shows that the maximum plunging force required at a rate of 20 mm/min is 14 kN while for the 60 mm/min plunging rate is 19 kN. It also shown that lower forging forces are experienced at 20 mm/min.

Plunging rate of 20 mm/min produced higher heat input to the weld compared to 60 mm/min plunging rate, because 20mm/min plunging rate takes longer time. Higher heat

input will result in higher temperature distribution and more material plasticization that facilitates the forging process and leads to significant reduction in forging force. Figure 4.1 shows that lower forging forces were experienced at 20 compared to 60 mm/min plunging rate.

Figure 4.2 shows effect of rotational speed on forging force. Increasing of rotational speed corresponds to significant reduction on maximum forging force experienced during the process according to hypothesis testing which showed that the P-value is less than 0.05 where P is the probability distribution of F statics in the non-parametric test. The maximum forging force at 1200 rpm, 60 mm/min and 4 seconds is 22.3 kN while it reduces to 19.4 kN at 1200 rpm for the same plunging rate and dwell time. This reduction in forging force results from higher heat input at the higher rotational speed.

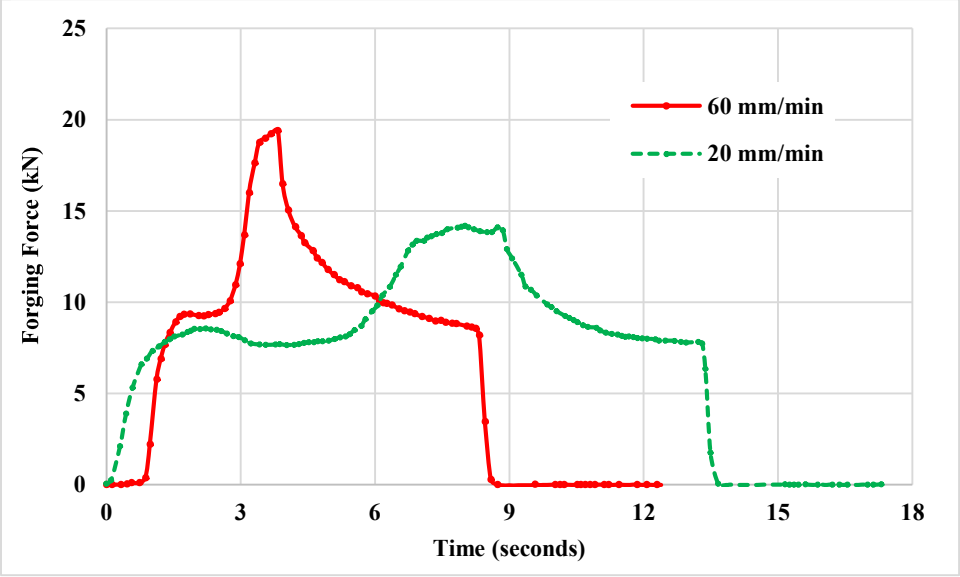

Figure 4.1: Effect of Plunging Rate on Forging Force for N=1200 rpm, and DT= 4 seconds

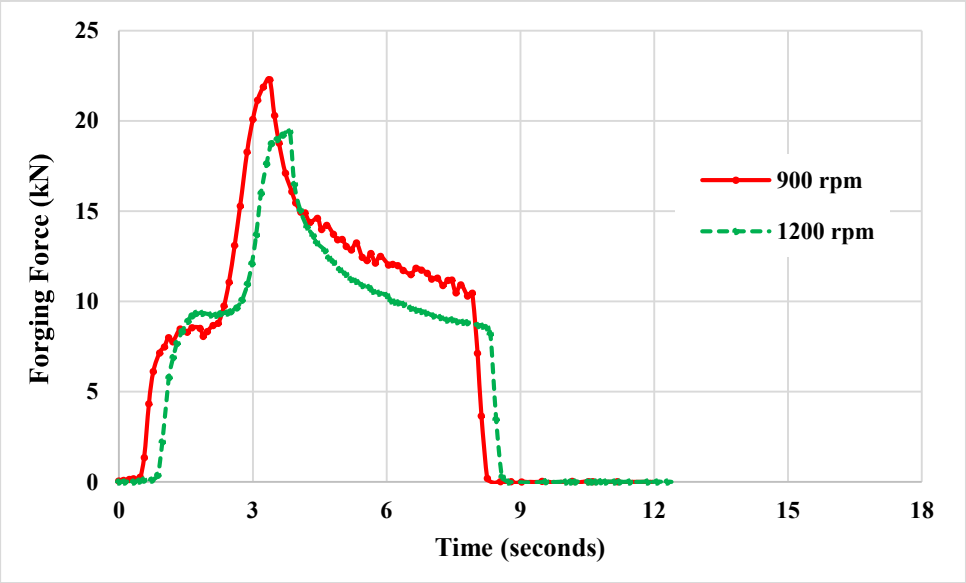

Figure 4.2: Effect of Rotational Speed on Forging Force for V=60 mm/min, and DT=4 seconds

Forging forces for 1200 rpm and 60 mm/min at two different dwell times of 2 and 4 seconds are shown in Figure 4.2. Increasing the dwell time showed almost no significant effect on the maximum forging force experienced at 1200 rpm and 60 mm/min. T-test for the effect of rotational speed on the forging force resulted in P-value greater than 0.05 which supports the claims that increasing the dwell time is not affecting the maximum forging force. Increasing the dwell time means allowing stirring phase to take longer time resulting in higher heat input to the weld. Zhang *et al.* [58] pointed out that rotational speed and dwell time are predominant factors of heat input to the weld. So increasing the dwell time would not affect the maximum forging force experienced during the welding. Dwell time may significantly affect heat input to the weld and weld quality and peak temperature experienced during welding. Effect of dwell time on forging force experienced by the pin tool is shown in Figure 4.3.

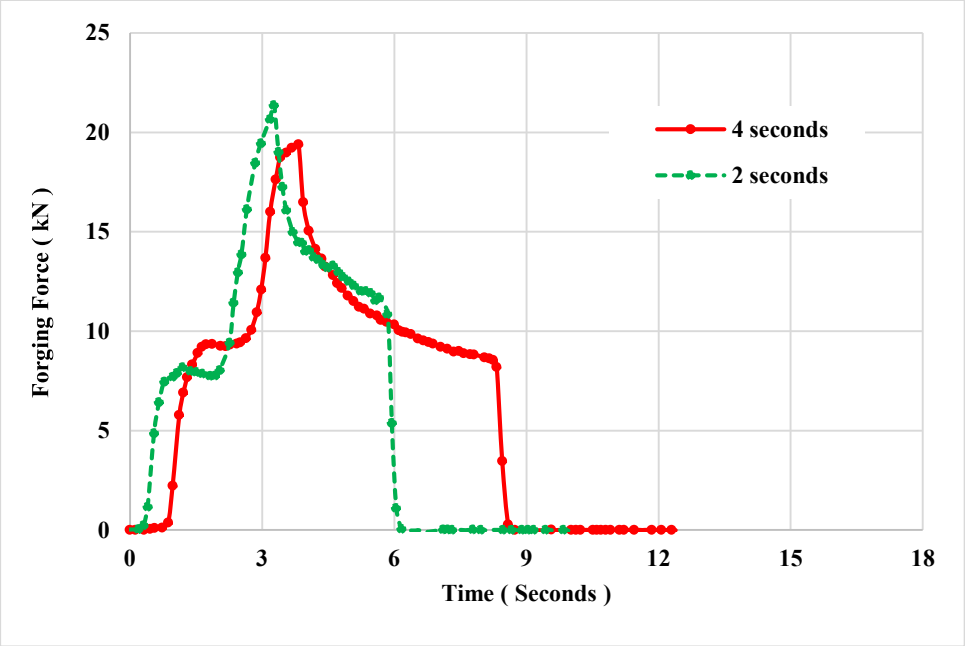

Figure 4.3: Effect of Dwell Time on Forging Force for N=1200 rpm and V=60 mm/min

4.2 Microstructural Analysis

The microstructure analysis of the FSSW cross-sections specimen showed four microstructural regions. Figure 4.4 shows the average grain size at different microstructural regions for the FSSW welds produced using a threaded pin tool at a rotational speed of 900 rpm, plunging rate of 20 mm/min and 2 seconds dwell time.

The base metal microstructure is shown in Figure 4.5a. Figure 4.5b shows very fine microstructure on the Stir Zone (SZ) of the welded specimen. A very fine microstructure is resulted from mechanical working and dynamic recrystallization during FSSW process [15, 58, 59].

Thermo-Mechanically Affected Zone (TMAZ) is located between the SZ and HAZ. This zone has a little bit coarser microstructure compared to SZ microstructure and finer

microstructure than the heat affected zone (HAZ). The TMAZ microstructure is shown in Figure 4.5c. The Heat affected zone is surrounding the SZ. This region is only affected by the thermal cycle, which results in grain coarsening due to self-annealing effect. Figure 4.5d shows the (HAZ). The HAZ microstructure is coarser than the base metal microstructure. The HAZ is not affected by mechanical working because it is far from the welding center.

Varying the welding parameters is affecting the grain size in these affected zones. Increasing of heat input results in grain coarsening and consequently increase of the average grain sizes in these zones, while reduction of heat input to the weld results in grain refinement and reduces average grain size of welded samples.

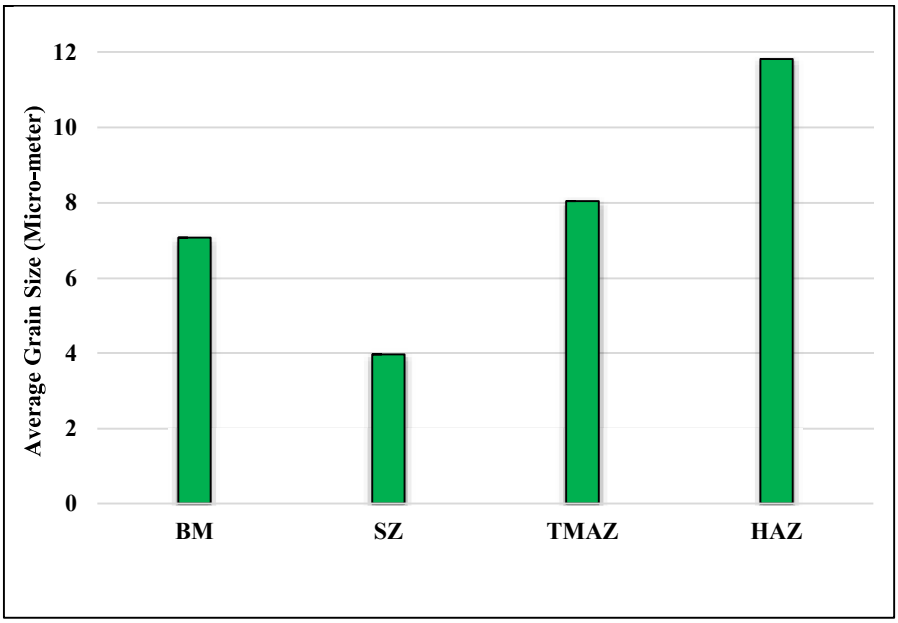

Figure 4.4: Microstructural Zones Grain Size of Threaded Pin Tool at N=900 rpm, V= 20 mm/min and DT=2 seconds

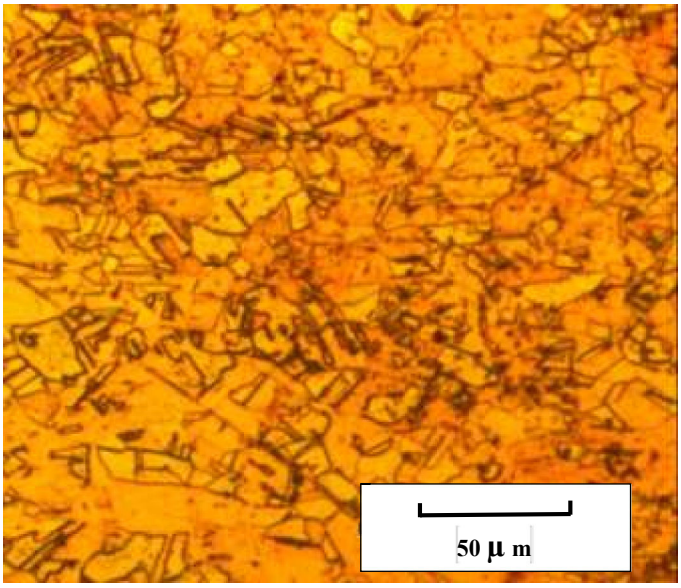

(a) Base Metal (BM)

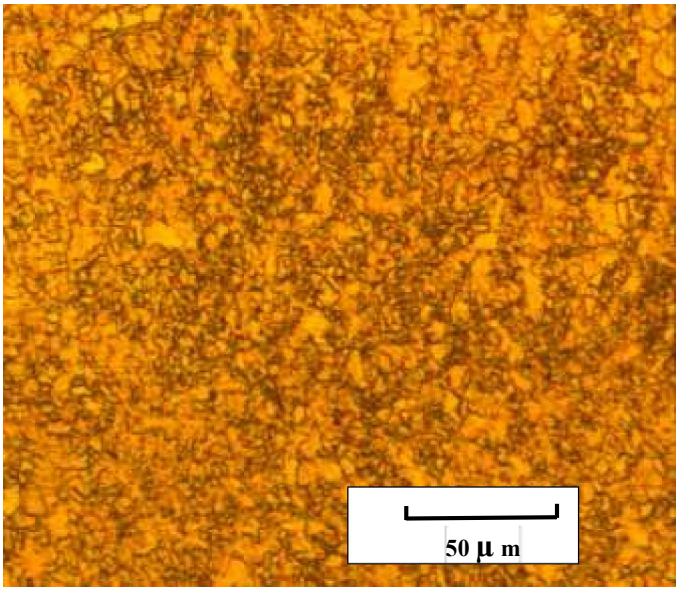

(b) Stir Zone (SZ)

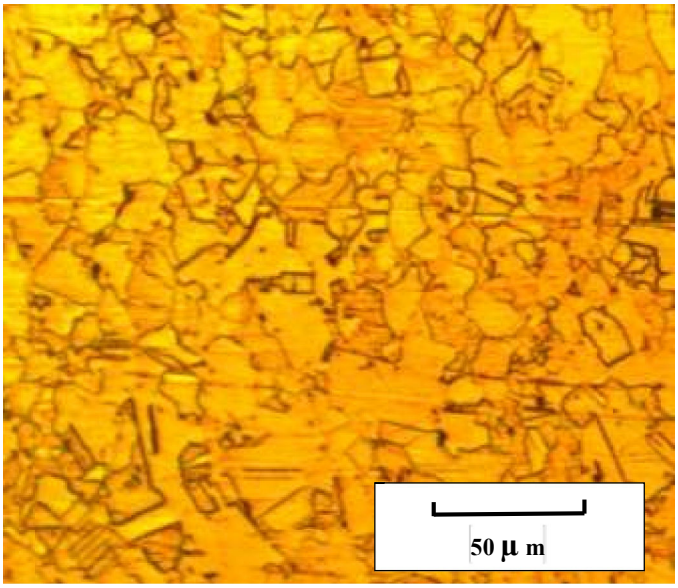

(c) Thermo-Mechanically Affected Zone (TMAZ)

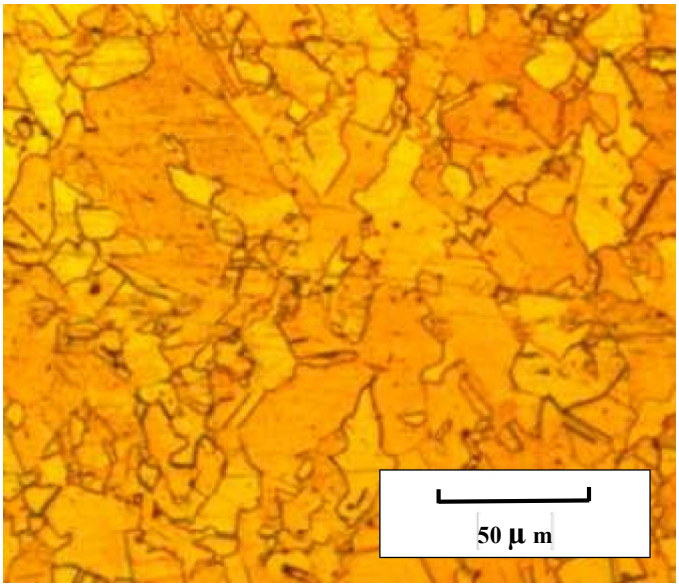

(d) Heat Affected Zone (HAZ)

Figure 4.5: Microstructural Zones on Friction Stir Spot Welds Produced at 900 rpm, 20 mm/min and 2 seconds Using Threaded Pin Tool

4.3 Evaluation of Weld Joint Quality

Three metallurgical parameters were studied to evaluate the FSSW welds. These parameters are hook formation quality, effective upper sheet thickness, and complete bonding region area. Figure 4.6 shows metallurgical bonded regions, hook and effective upper sheet thickness at 900 rpm rotational speed, 20 mm/min plunging rate and 2 seconds dwell time.

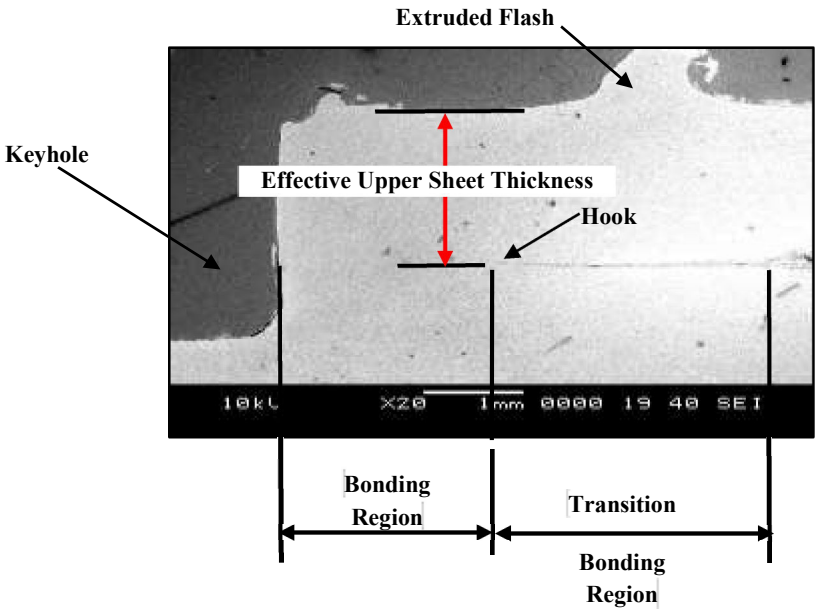

Figure 4.6: SEM Micrograph of Metallurgical Bonded Regions, for N=900 rpm, V=20 mm/min, DT = 2 seconds

4.3.1 Weld Joint Quality on the Hook Feature

Scanning Electron Microscopy (SEM) analysis was carried out on the hook feature (end of the transition region) to investigate the effect of welding parameters on quality of the weld at the hook in terms of existing of cracks and voids.

This region is a critical one, where cracks resulting from applying external loads initiate, and then propagate through the sheet thickness or along sheets interface. This observation is in agreement to what has been highlighted by Wang *et al.* [34].

Figure 4.7 and Figure 4.8 show the end of transition region (also called hook) for 1200 rpm, 20 mm/min, 2 seconds and 4 seconds dwell time, respectively. Both micrographs show end of transition region that is free of voids and cracks. The effect of increasing the dwell time from 2 seconds to 4 seconds results in a formation of white bubbles. These bubbles are expected to form under high pressure and heat input.

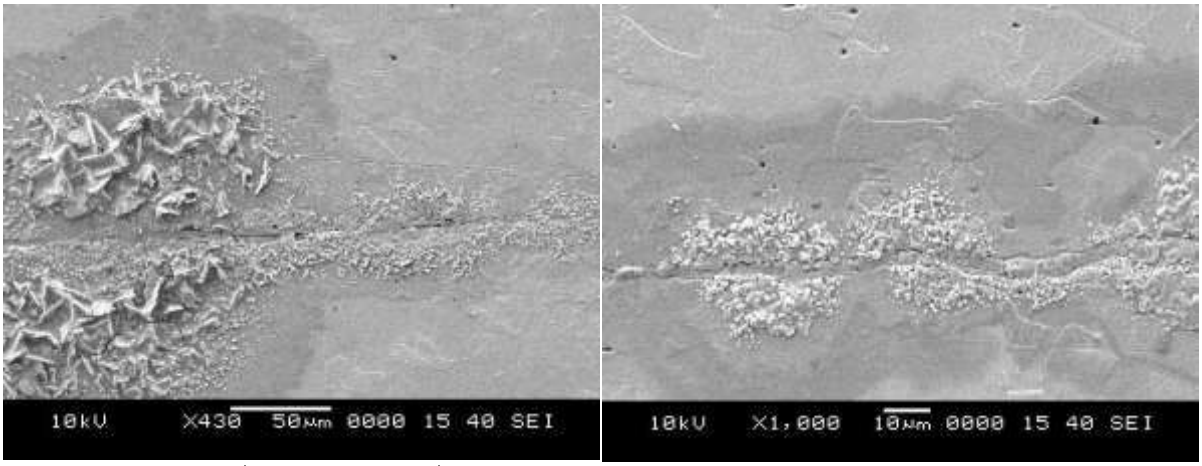

(a) Over look view (b) **Higher Magnification**

Figure 4.7: SEM Micrographs for the End of Transition Region at N=1200, V=20 mm/min, DT=2 Seconds

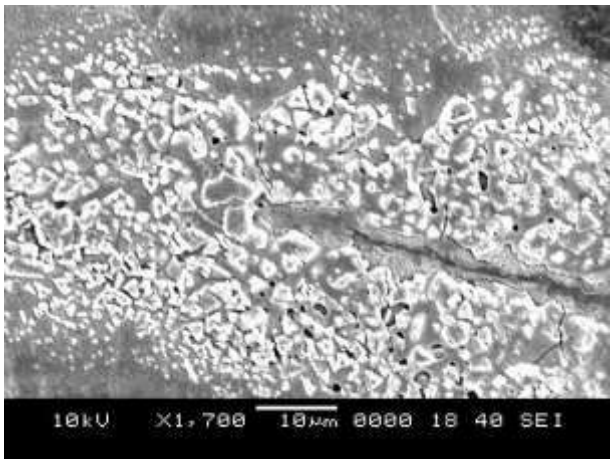

Figure 4.8: SEM Micrographs for the End of Transition Region at N= 1200 rpm, V=20 mm/min, DT=4 seconds

Figure 4.9a and Figure 4.9b show transition region and hook feature respectively, at 900 rpm, 20 mm/min and 2 seconds. Isolated voids were formed along the transition region with absence of white bubbles. Absence of white bubbles proved that for lower level of heat input (i.e. 900 rpm rotational speed) the white bubbles will not form.

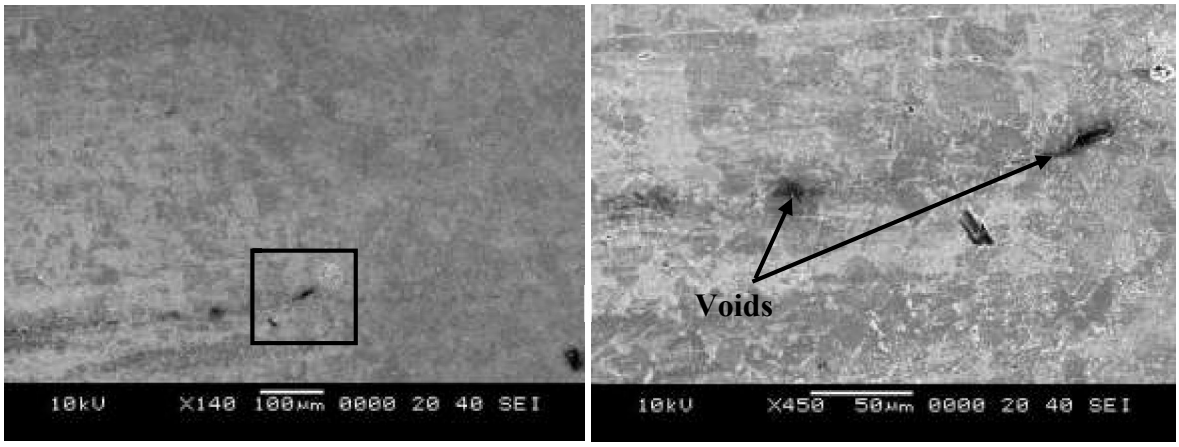

(a) End of Transition Region **(b) Higher Magnification**

Figure 4.9: SEM Micrographs at N=900 rpm, V= 20 mm/min DT = 2 seconds

Hook formation was observed for 1200 rpm, 60 mm/min and 2 seconds as shown in Figure 4.10a. Cracks and voids at the end transition region were observed. This hook feature facilitates cracks initiation and propagation. Figure 4.10b shows the end of transition region for 1200 rpm, 60 mm/min and 4 seconds. Smooth end transition region with presence of isolate voids along the end of transition region was observed, as shown in Figure 10.b. Tensile shear strength analysis showed relatively lower tensile shear strength for all rotational speeds with 60 mm/min plunging rate, and 2 seconds dwell time (mean of the tensile weld strength is less than 3.65 kN). Mean of the tensile weld strength of 5.45 kN was recorded for 1200 rpm, 60 mm/min and 4 seconds dwell time.

Smooth end transition region, free of voids was observed at 1200 rpm, 20 mm/min and 2 seconds dwell time as shown in Figure 4.7. Increasing the dwell time from 2 to 4 seconds for the same rotational speed and plunging rate did not manifest any enhancement of weld quality. However, the amount of white bubbles around the transition region has increased. High plunging rate of 60 mm/min did not deliver sound weld for 2 seconds dwell time. Increasing dwell time to 4 seconds in case of 60 mm/min plunging rate enhanced the quality of transition bonding region, leading to an increase in tensile shear strength of 5.45 kN.

In summary, the analysis of hook feature revealed that the quality of the hook can give an indication for the weld strength. Absence of cracks and voids indicates high weld strength while hook feature with cracks, voids indicates the opposite.

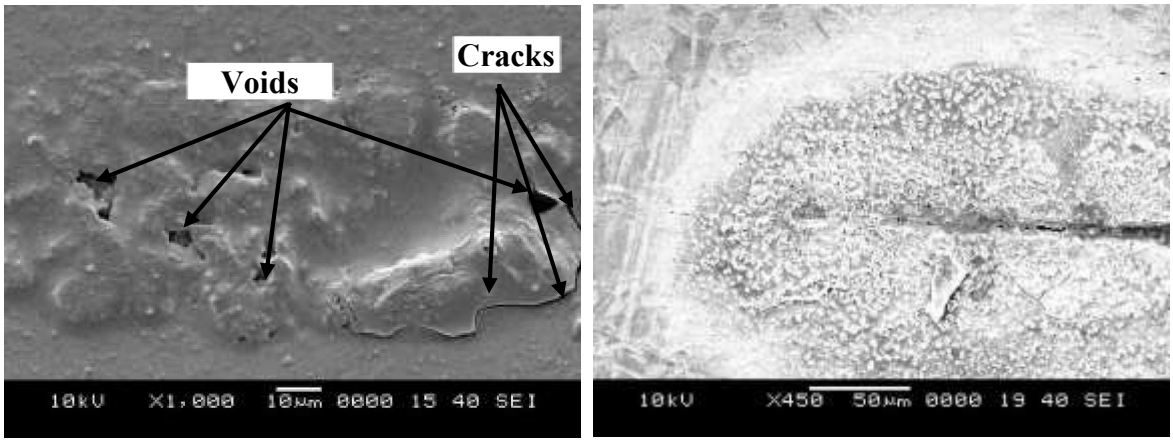

(a) DT = 2 seconds **(b) DT = 4 seconds**

Figure 4.10: SEM Micrographs at N=1200 rpm, V= 60 mm/min

4.3.2 Effective Upper Sheet Thickness Analysis

Effective upper sheet thickness is the distance from hook tip to top surface of upper sheet as shown in Figure 4.6. Figure 4.11 shows effective upper sheet thickness for different welding parameters. According to Figure 4.11a to Figure 4.11c high plunging rate

pushes the hook downward so that the effective upper sheet thickness is greater than 2 mm (2.0 mm is the upper sheet thickness). On the other hand, hook goes upward for 20 mm/min plunging rate as shown in Figure 4.11d and Figure 4.12 a,c and d. Material flow during the welding process influences the hook formation whether it goes upward or downward.

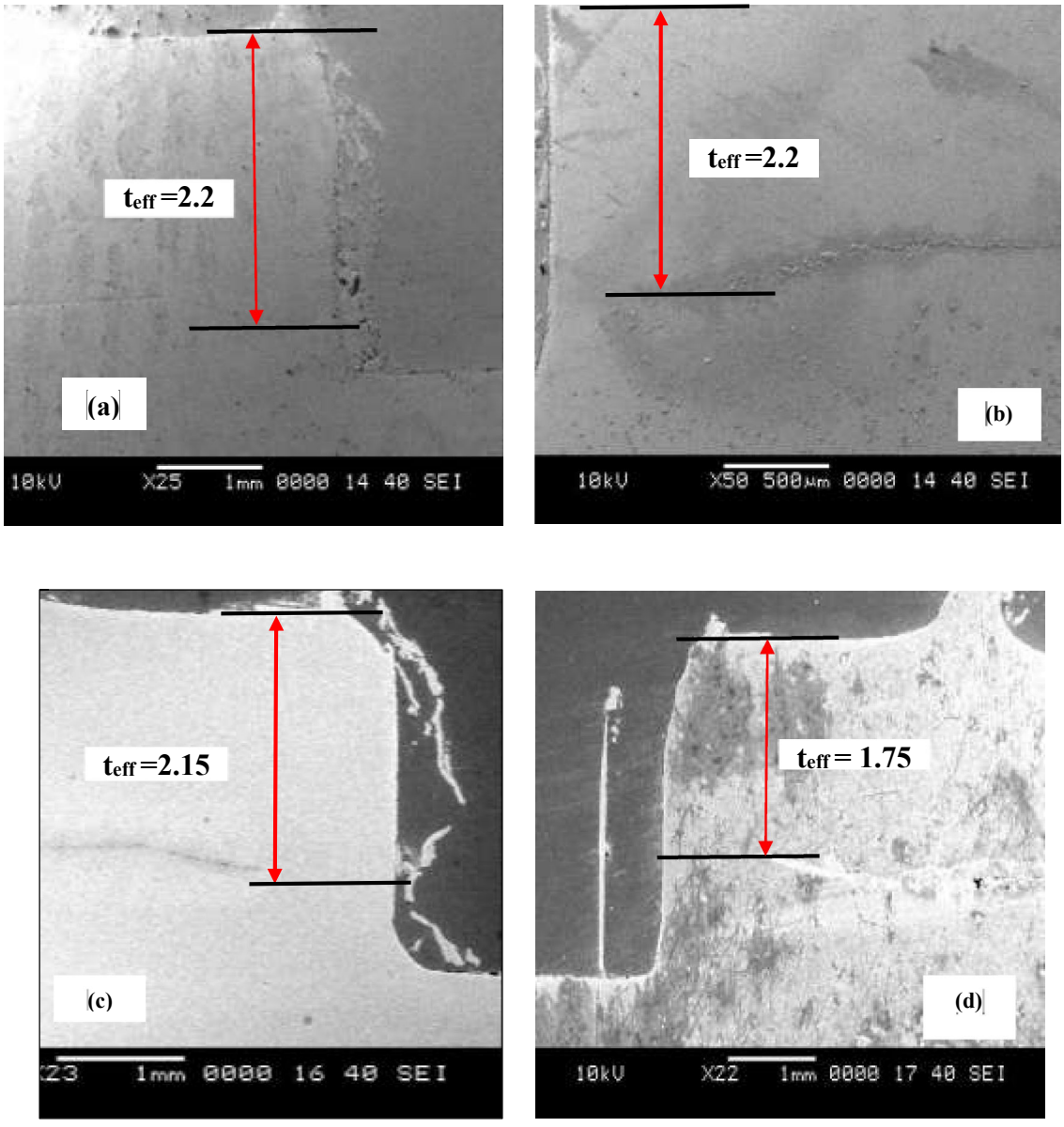

Figure 4.11: Effective Upper Sheet Thickness, (a) N=1200 rpm, V=60 mm/min, DT=2 seconds-Left, (b) N=1200 rpm, V=60 mm/min, DT=2 seconds-Right, (c) N=900 rpm, V=60 mm/min, DT=2 seconds, (d) N=1200 rpm, V=20 mm/min, DT=4 seconds

Yuan *et al.* [2] pointed out that the strength of the FSSW welds depends on size of bonding region, hooking feature, and effective thickness of the upper sheet. They concluded that higher effective upper sheet thickness indicated higher tensile shear strength. Badarinarayan *et al.* [11] studied the effect of tool geometry on hook formation. They have shown that tool geometry significantly affects hook formation and effective upper sheet thickness as shown in Figures 4.11 and 4.12 and hook feature is attributed to the material flow during the welding process. They also found that increasing of effective upper sheet thickness increases the tensile shear strength of the weld. They also have shown that crack initiation and propagation are determined by bonded region size, material properties and stress concentration. Large effective upper sheet thickness (larger than 2.0 mm) at 60 mm/min plunging rate resulted in low tensile shear strength below 3.5 kN. Smaller effective upper sheet thickness for 20 mm/min plunging rate welds, obtained relatively higher welds strength more than 4.5 kN compared to 60 mm/min plunging rate. However, no direct relationship was found between effective upper sheet thickness and tensile shear strength as reported by Badarinaryan *et al.* [11].

According to experimental observations, hook formation is affected by material flow during the process. Heideman *et al.* [46] highlighted the importance of material flow from lower sheet to the upper one to produce a sound weld with high tensile shear strength. This was also reported by Yang *et al.* [15] who proposed an experimental material flow model for FSSW. Flowing of the material from lower sheet to the upper one enhanced material flow and consequently improved weld joint strength. However, flowing of the material from the lower to the upper sheet moves the hook upward towards the upper sheet [15]. Hook moving upward reduces effective upper sheet thickness. It indicates better

material flow that results in better weld strength. This contradicts Heideman *et al.* [46] who highlighted the direct relation between the weld strength and the effective upper sheet thickness. This contradiction may have resulted from analysis of different materials.

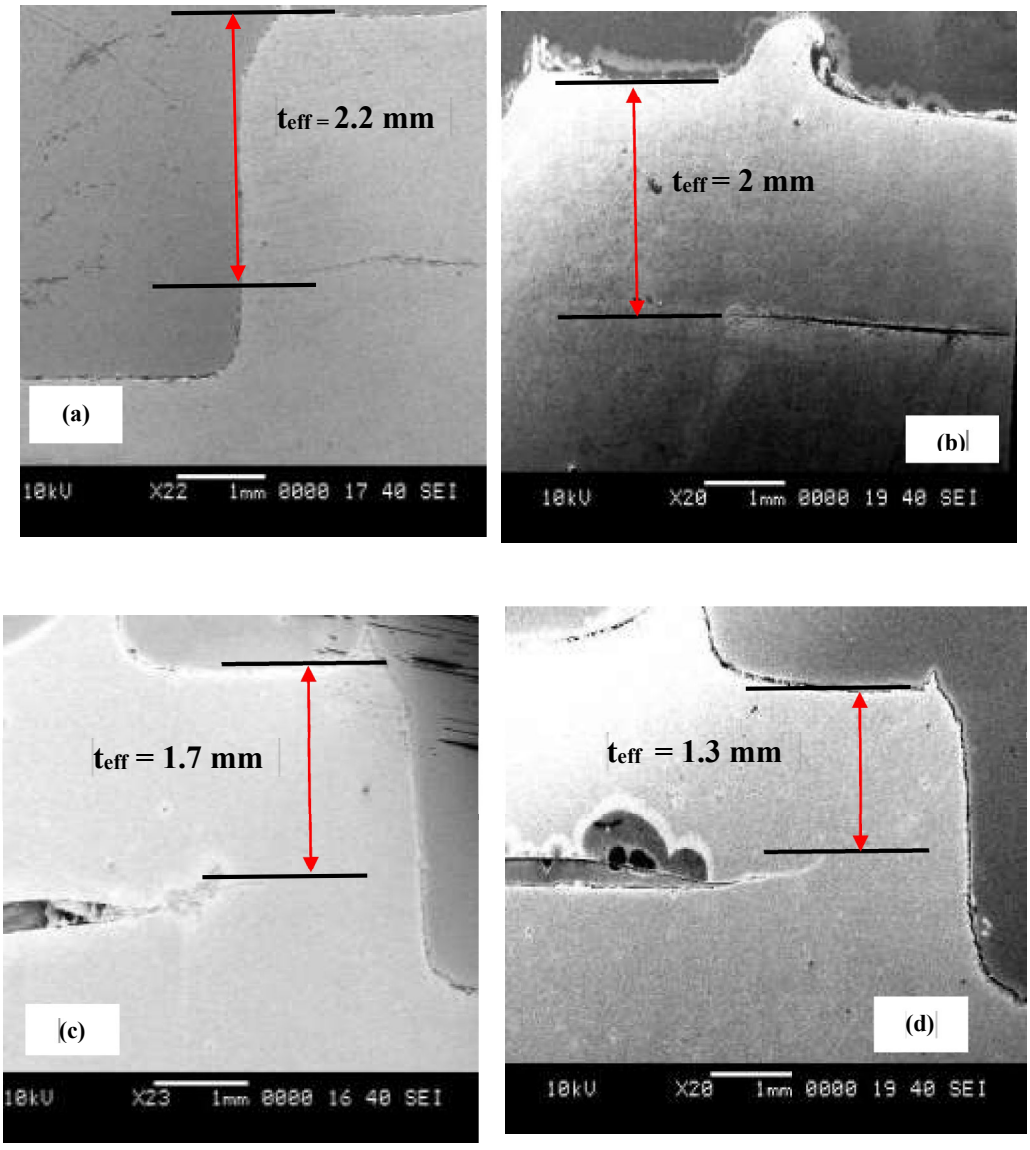

Figure 4.12: Effective Upper Sheet Thickness, (a) N=900 rpm, V=60 mm/min, DT=4 seconds, (b) N=1200 rpm, V=60 mm/min, DT=4 seconds, (c) N=900 rpm, V=20 mm/min, DT=2 seconds-Threaded, and (d)) N=900 rpm, V=20 mm/min, DT=4 seconds-Threaded

In conclusion, the effective upper sheet thickness can give indication for the material flow during the process. Bonding region area may have significant effect on the weld strength. Similar observation was reported by Yuan *et al.* [2].

4.3.3 Metallurgical Bonding Region Area Analysis

The optical microscope and micrometers in x and y directions that were embedded with the micro-hardness tester machine were utilized in measuring the bonding region size for each set of welding parameter. Complete Bonding Region Size (CBRS) is measured from the hook tip to the keyhole edge, then Complete Bonding Region Area (CBRA) in mm^2 is the annulus area which can be calculated by considering the keyhole area using the following equation.

$$CBRA = \pi \times [(CBRS + 2.5)^2 - 2.5^2] \quad (4.1)$$

This data was used to investigate the effect of welding parameters on bonding region size. Complete metallurgical bonded region and hook feature of friction stir spot cross-section as shown in Figure 4.6 and Table 4.1 shows bonded region size.

Table 4.1 Bonding Region Size

Simple Pin Tool						
Experiment No.	N [rpm]	V [mm/min]	DT [seconds]	Mean of Tensile Shear Strength [kN]	Complete Bonding	
					Left [mm]	Right [mm]
1	900	60	2	3.15	1.12	1.3
2	900	60	4	4.4	0.61	0.53
3	900	20	2	3.25	1	0.95
4	900	20	4	4.4	2.5	2.4
5	1200	60	2	3.65	0.34	0.47
6	1200	60	4	5.45	2.35	2.1
7	1200	20	2	5.55	1.35	1.36
8	1200	20	4	5.15	1.7	1.72
Threaded Pin Tool						
1	900	20	2	7.115	1.56	1.56
2	900	20	4	7.075	2	2

Figure 4.13 shows main effect plot of complete bonded region output. From this figure, it can be concluded that rotational speed has almost no significant effect on bonded region area.

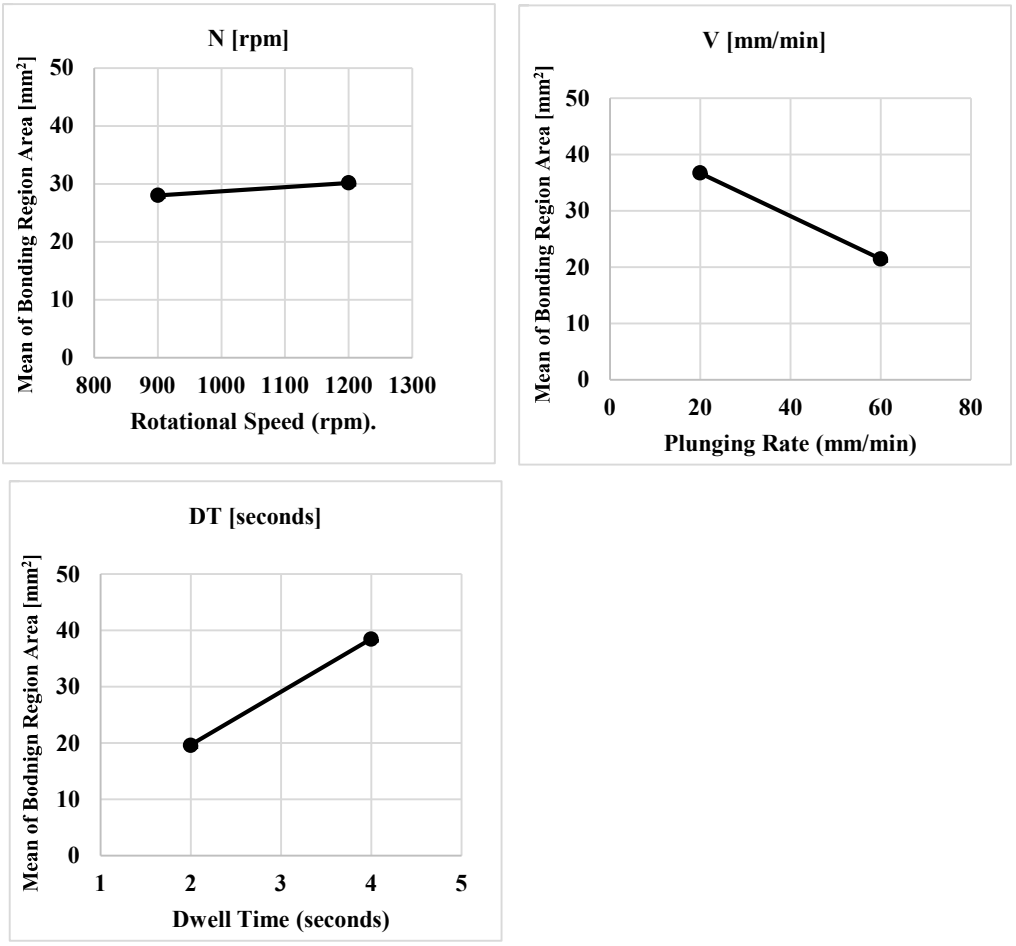

Figure 4.13: Main Effect Plot of Welding Parameters on Bonding Region Area

These results can be verified from the Vickers micro-hardness profile for the effect of rotational speed as shown in Figure 4.14. The steep reduction in hardness profile is attributed to transition region zone. This steep reduction occurred at the same distance from the weld center, which means that increasing of rotational speed has no significant effect

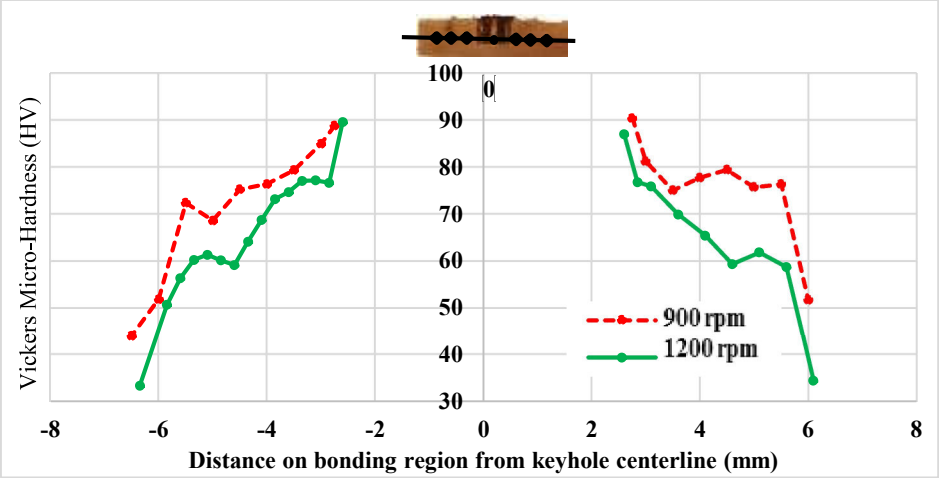

Figure 4.14: Effect of Rotational Speed Variation on Vickers Micro-Hardness Profile on Sheets Interface at V=20 mm/min, DT=2 Seconds Using Simple Pin Tool

on bonding region. Steep reduction in the micro-hardness profile at sheets interface indicates measuring the hardness on partial bonded region where voids start to exist. According to Figure 4.14 steep reduction occurred at the same distance from the weld center for both rotational speed, which means that rotational speed has no significant effect on varying bonding region area. In addition, ANOVA analysis shown in Table 4.2 confirms that rotational speed has no significant effect on bonding region area because it has the highest P-value that is greater than 0.05.

Table 4.2 P-values from Analysis of Variance of DoE parameters of Bonding Region Area Output

Welding Parameters	P: Probability Distribution
Rotational Speed N [rpm]	0.89
Plunging Rate V [mm/min]	0.44
Dwell Time DT [seconds]	0.37

Figure 4.15 shows weld parameters interaction plot for bonded region area output. It is clearly shown that rotational speed has no significant effect on bonded region area. Conversely, dwell time and plunging rate are significantly affecting the bonded region area.

Increasing the dwell time resulted in increase of the bonded region area as shown in main effect plot on Figure 4.13. These results are in agreement with the micro-hardness profile along the interface because increasing the dwell time from 2 to 4 seconds resulted in wider area before micro-hardness steep reduction compared to 2 seconds dwell time at 1200 rpm, 60 mm/min plunging rate as shown in Figure 4.16. Interaction plot on Figure 4.15 also shows that dwell time is increasing bonded region area regardless of rotational speed and plunging rate.

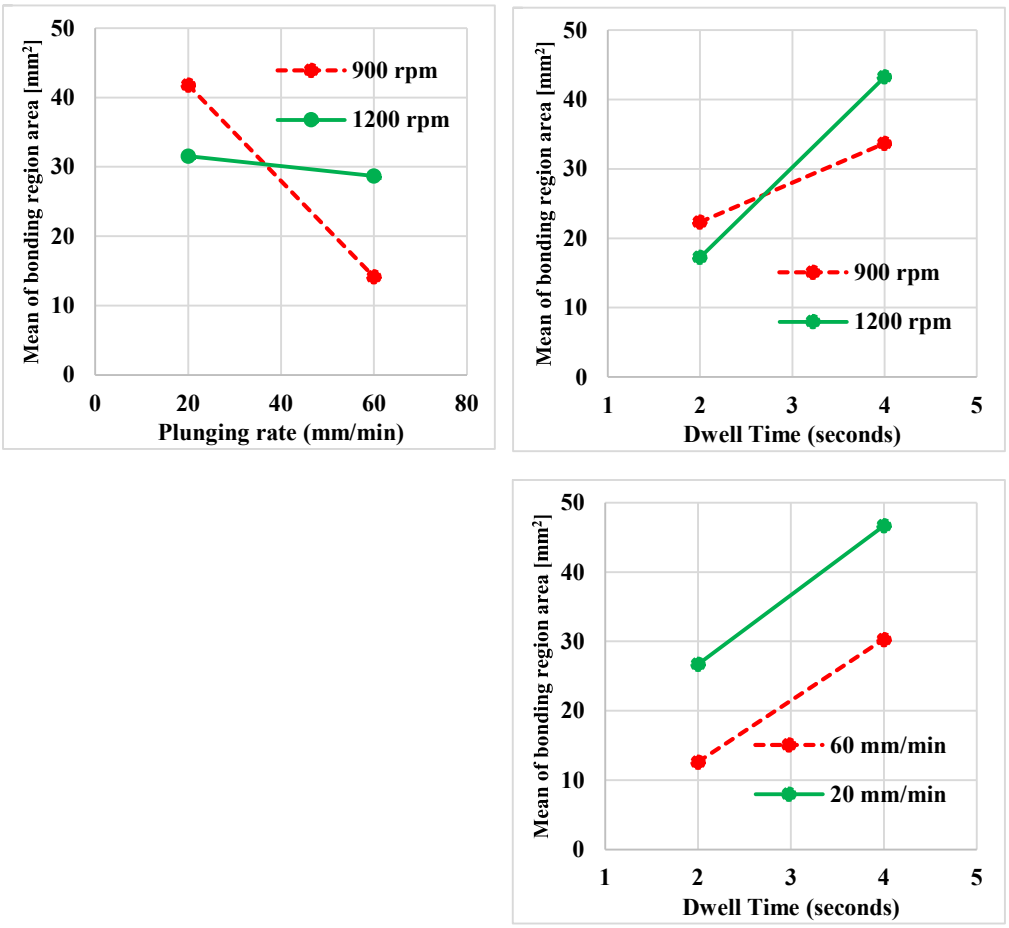

Figure 4.15: Interaction Plot for the Effect of Welding Parameters in Bonding Region Area for Simple Pin Tool

On the other hand, increasing the plunging rate reduced the bonded region area as shown in Figure 4.13. Welds that were produced at 20 mm/min plunging rate have higher

bonded region area for all dwell times. This is in conformance with micro-hardness profile on sheets interface results as shown in Figure 4.17.

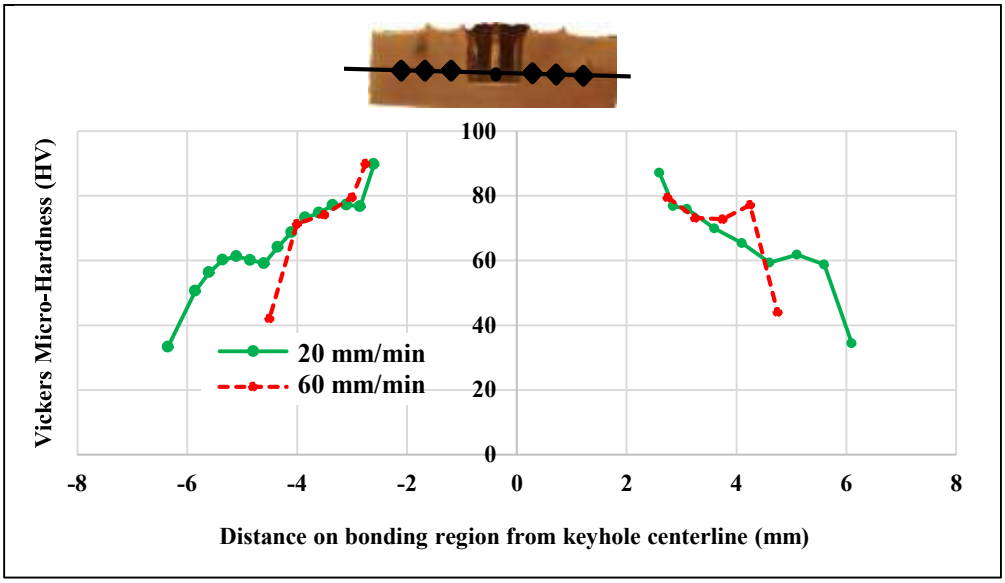

Figure 4.16: Effect of Dwell Time on Vickers Micro-Hardness Profile in Sheets Interface at N=1200 rpm and V = 60 mm/min Using Simple Pin Tool

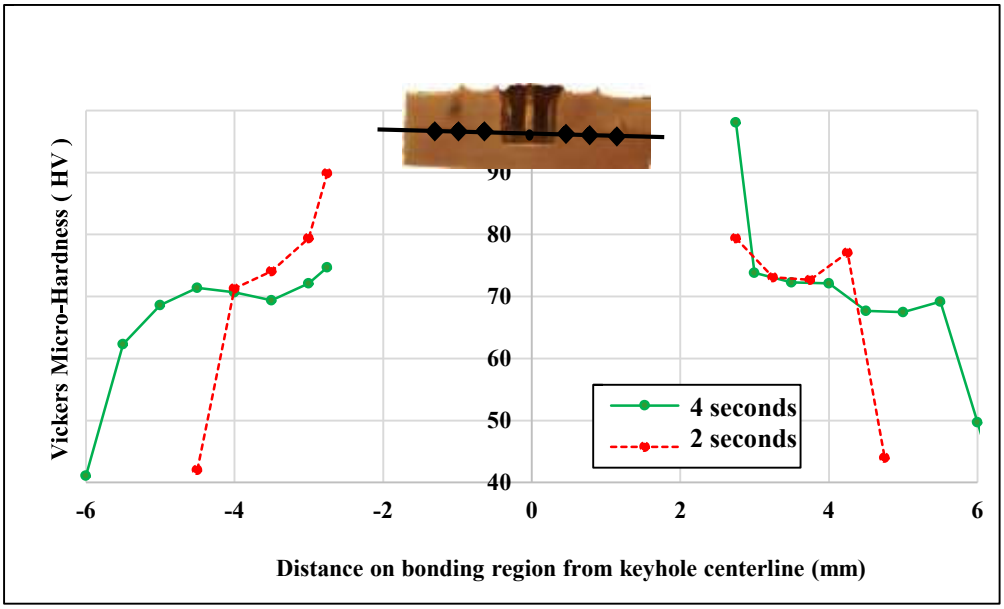

Figure 4.17: Vickers Micro-Hardness Profile in Sheets Interface at N=1200 rpm and DT=2 seconds, Using Simple Pin Tool

Badarinarayan *et al.* [11] pointed out that bonded region area is the area that carries the load. The authors reported that this area is one of the parameters that influences FSSW welds strength. From Table 4.1 it's clearly seen that increase of bonding region often resulting in higher tensile weld strength. This finding is similar to the observation reported by Badarinarayan *et al.* [11].

4.4 Tensile Shear Strength Analysis

Tensile shear strength is carried for the simple tool full factorial design of experiments as shown in Table 3.6. To investigate the effect of pin tool geometry the experiment matrix Table 3.7 was considered.

4.4.1 Full Factorial Design of Experiment

Full factorial design of experiment is implemented for rotational speed, plunging rate and dwell time, using a simple pin tool. Minitab® is used for the analysis of factorial design of experiment as illustrated in Table 3.6.

The main effect plot of design of experiment parameters for tensile shear strength output is shown in Figure 4.18. It is clearly shown that weld joint tensile shear strength is increasing with increase of rotational speed for all plunging rate and dwell time considered. Cox *et al.* [60] studied the effect of rotational speed on FSSW of Aluminum alloy. The highest tensile shear strength was obtained at 750 rpm rotational speed. Increase of rotational speed to 2000 rpm decreased weld strength. They concluded that decreasing of rotational speed results in higher weld strength, which is in contradiction to the finding of this investigation. This controversy could be attributed to the different welding parameters

and different materials used for welding. Heat input to the weld is influenced by the material properties of the work-piece being welded.

Analysis of variance (ANOVA) of experiment was conducted by taking 5% confidence interval. Table 4.3 shows P-value according to ANOVA analysis for the effect of welding parameters on tensile shear strength. According to Table 4.3, rotational speed has the most significant effect on tensile shear strength of the joint, followed by dwell time while plunging rate has no significant effect because its P-value is higher than 0.05.

Table 4.3 P-values from Analysis of Variance of DoE Parameters of Tensile Shear Strength Output

Parameters	P: Probability Distribution
Rotational Speed N [rpm]	0.01
Plunging Rate V [mm/min]	0.073
Dwell Time DT [seconds]	0.014

Heideman *et al.* [46] found that the rotational speed has the most significant effect on tensile shear strength when it increases from 1000 to 2000 rpm. They also found that rotational speed has no significant effect when it increased from 2000 to 3000 rpm. This may be resulted because adequate heat input is produced at 2000 rpm rotational speed more increase on heat input will has no significant effect on weld strength.

On the other hand, Zhang *el al.* [58] pointed out that grain coarsening resulted from high heat input at high rotational speed decreases joint strength. However, increasing of rotational speed in this study increased heat input to the weld as well as weld joint tensile shear strength. This controversy may be attributed to the rotational speed under study and material properties. High rotational speed increases heat input as well as plasticization

under the pin, allowing better material flow and voids free welds according to Galvão *et al.* [44].

Increasing of plunging rate from 20 to 60 mm/min decreases the mean of the tensile shear strength from 4.6 to 4.2 kN. Increasing dwell time from 2 to 4 seconds increases the mean of tensile shear strength from 4.2 to 4.6 kN as shown in Figure 4.18.

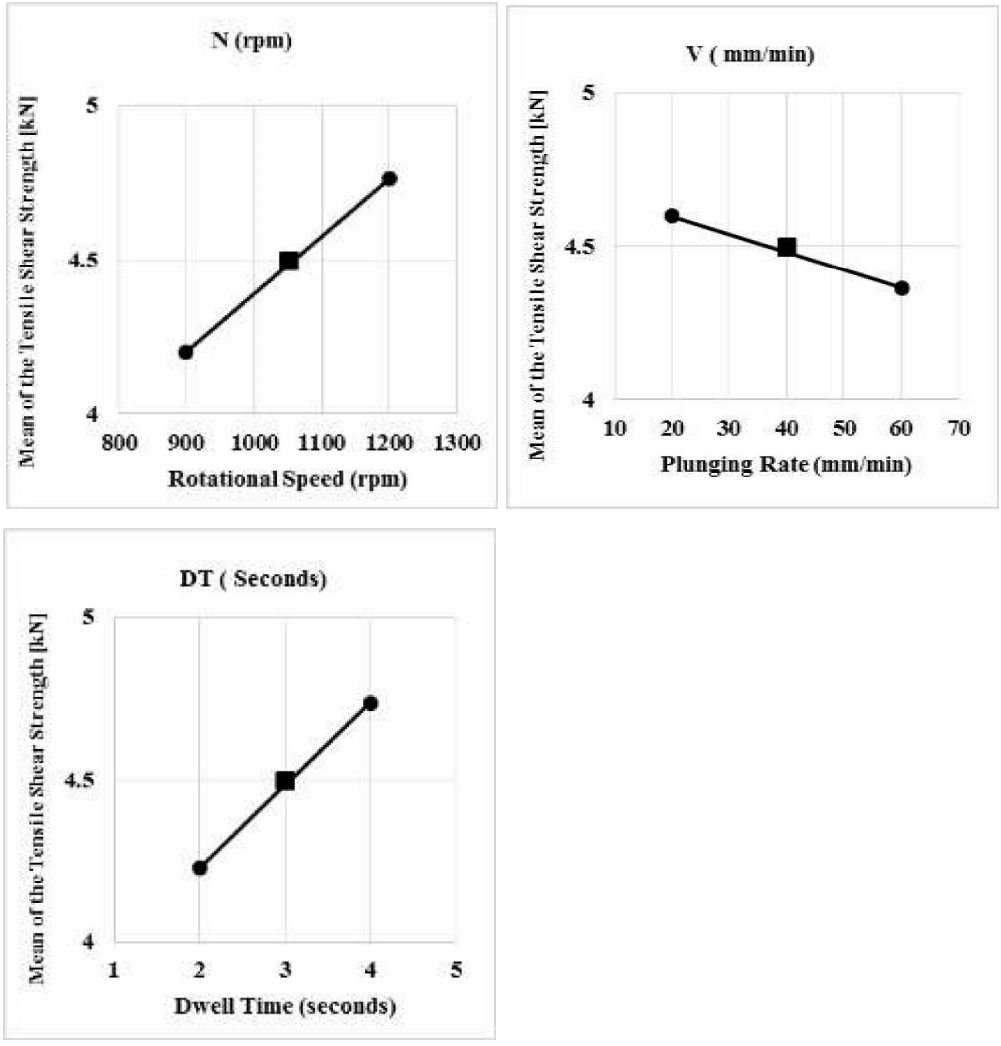

Figure 4.18: Main Effect of Welding Parameters in Tensile Shear Strength Plot for Simple Pin Tool

Increasing plunging rate resulted in decrease of the tensile shear strength. The reduction in tensile shear strength is steeper for 1200 rpm case, because reduction in heat input at 1200 rpm is much higher than at 900 rpm as shown in Figure 4.19.

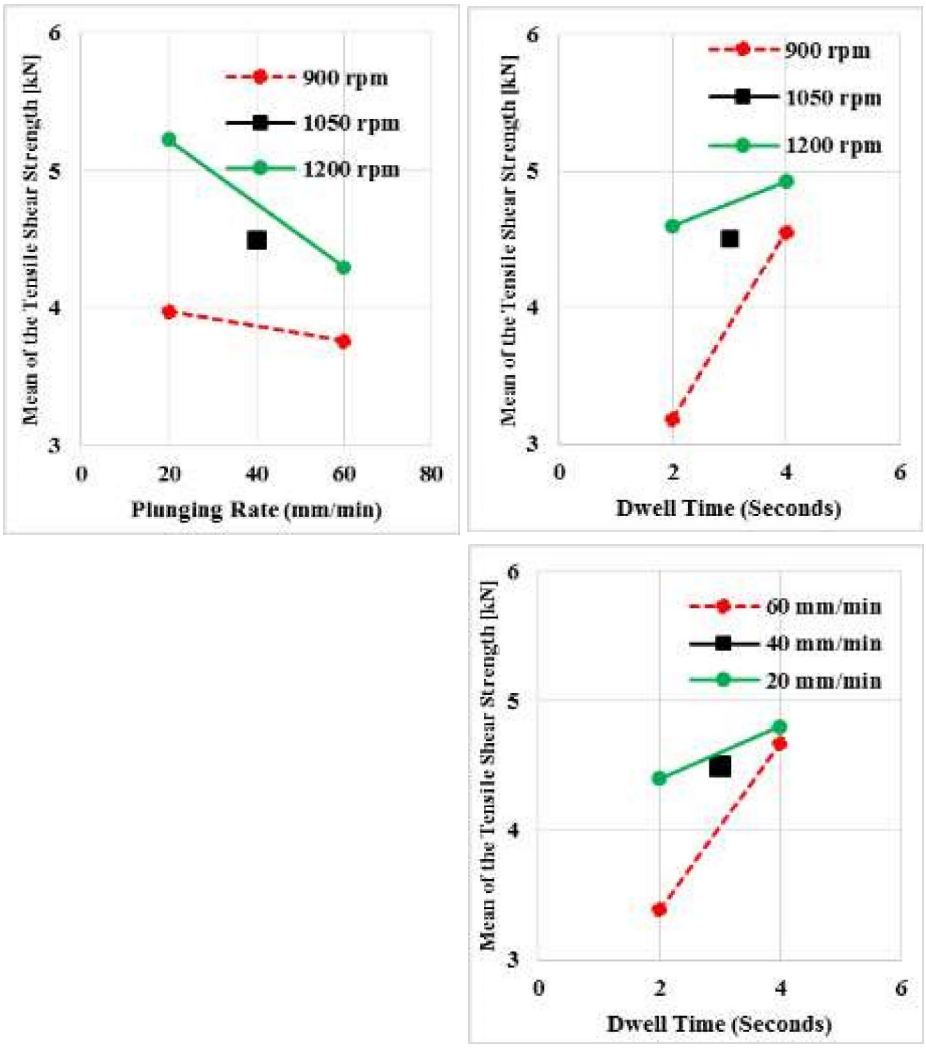

Figure 4.19: Welding Parameters Interaction Plot for the Simple Pin Tool

In summary, full factorial design analysis showed that rotational speed has the most significant effect on tensile shear strength of the weld joint. Increasing of rotational speed resulted in higher weld strength. Increasing the dwell time from 2 to 4 seconds has no

significant effect on increasing weld strength for 1200 rpm rotational speed and 20 mm/min plunging rate. This may be attributed to sufficient heat input to the weld for 1200 rpm, 20 mm/min and 2 seconds dwell time. Dwell time affected weld strength of 60 mm/min plunging rate significantly.

4.4.2 Effect of Pin Tool Geometry on Tensile Shear Strength

Figure 4.20 shows comparison between tensile shear strength analysis carried out for threaded and simple pin tool. Welding was performed at 900 rpm rotational speed, 20 mm/min plunging rate and 2 seconds dwell time for both pin tools. Threaded pin tool produced a weld having a tensile shear strength of 7 kN, while simple pin tool weld produced 3.5 kN tensile shear strength. Because threaded pin tool enhances material flow during welding, this resulted in a higher weld strength.

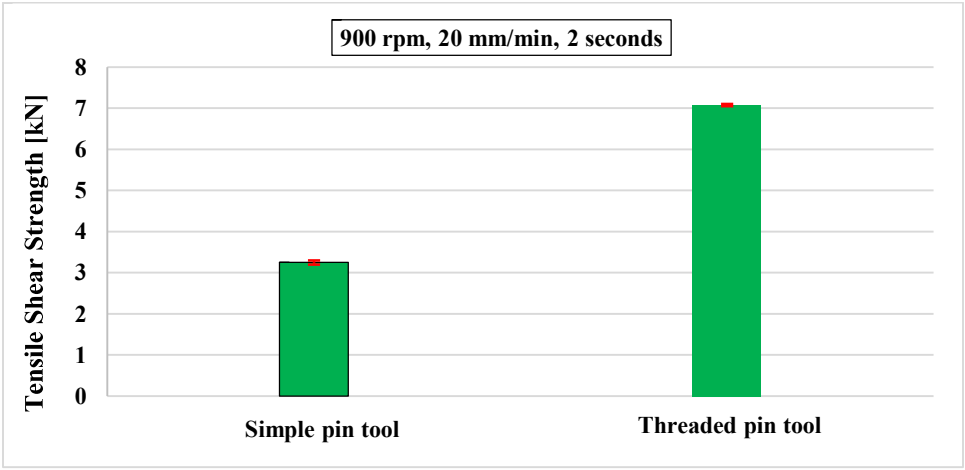

Figure 4.20: Effect of Pin Tool Feature on Tensile Shear Strength

4.4.3 Effect of Dwell Time on Tensile Shear Strength for the Threaded Pin Tool

Experimental testing for friction spot welds revealed that changing the dwell time from 2 to 4 seconds has shown no significant change in weld tensile shear strength using

threaded pin tool at 20 mm/min plunging rate and 900 rpm rotational speed. This may be attributed to sufficient heat input produced for 2 seconds dwell time. More heat input for 4 seconds dwell time has shown no significant effect on weld strength as depicted in Figure 4.21.

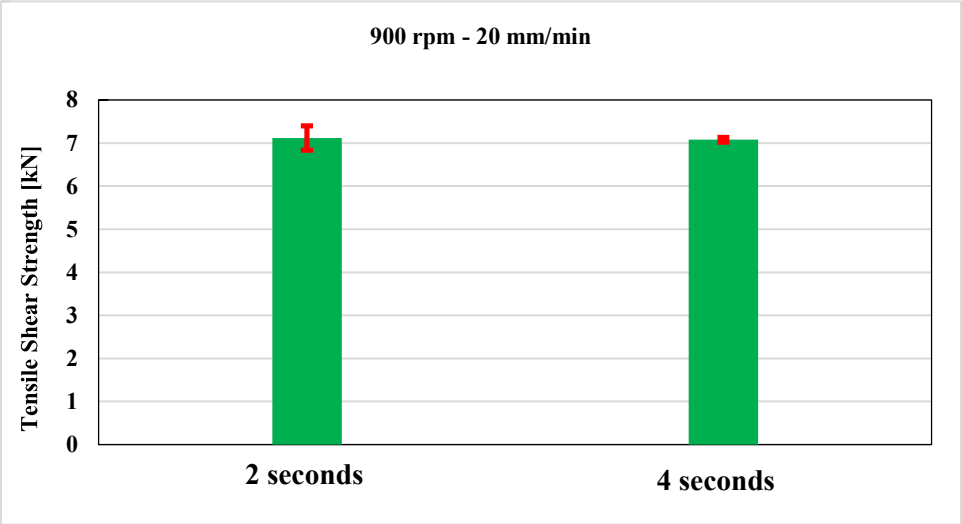

Figure 4.21: Tensile Shear Strength Results, N=900 rpm, V=20 mm/min using threaded pin tool

4.5 Fracture Surface Morphology Analysis

Scanning Electron Microscopy (SEM) analysis was carried out for fracture surface after tensile shear strength test to investigate the effect of welding parameters on the resulted fracture mode. For validation purposes of these results, tensile shear strength – Extension graph was consulted. All SEM micrographs were taken from a region that is very close to the keyhole, located in stir zone adjacent to the keyhole.

4.5.1 Effect of Dwell Time on Fracture Surface Morphology

Slip band surface morphology was observed on fracture surface of the welds performed using welding parameters of 900 rpm, 20 mm/min, 2 and 4 seconds dwell time.

This indicates shear fracture mode as shown in Figure 4.22a and Figure 4.22b, respectively. Moreover, tensile shear strength – extension plot was consulted for fracture mode analysis. As shown in Figure 4.23 both welds have low extension, because the load reduced sharply after it reached the maximum tensile shear strength indicating shear fracture mode. These results are in agreement with fracture surface morphology analysis.

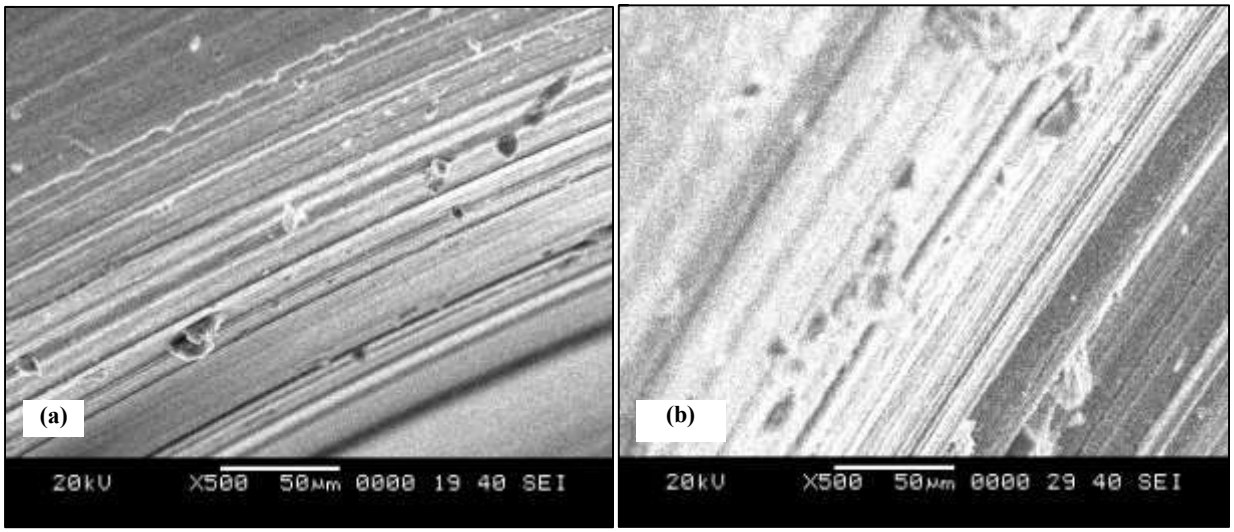

Figure 4.22: SEM Micrographs Fracture Morphology for (a) N=900 rpm, V=20 mm/min, DT=2 seconds and (b) N=900 rpm, V=20 mm/min, DT=2seconds

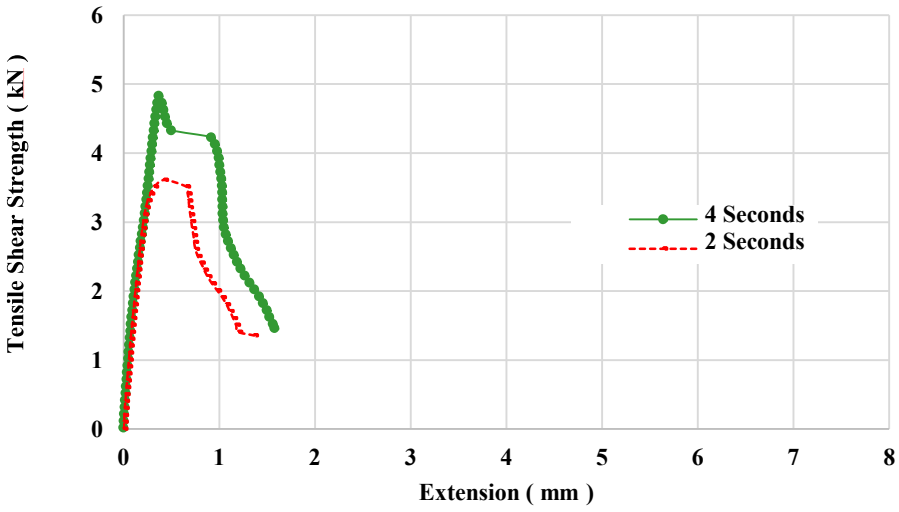

Figure 4.23: Tensile Shear Strength Extension Plot for N=900 rpm, V=20 mm/min, DT= 2 seconds

4.5.2 Effect of Rotational Speed on Fracture Surface Morphology

Figure 4.24a and Figure 4.24b show fracture surface morphology at 20 mm/min plunging rate, 2 seconds dwell time, for rotational speed of 1200 and 900 rpm, respectively. Slip band surface morphology, which is free of voids and dimples was observed on the welds that were produced at 900 rpm rotational speed. The SEM micrographs for 1200 rpm rotational speed welds show dimple like surface morphology with slip band surface. These dimples may be related to plasticity of the joint. The tensile shear strength extension graph in Figure 4.25 shows higher elongation before complete fracture is recorded at 1200 rpm welds. This could be associated to ductile failure mode. Heidarzadeh *et al.* [45] have shown that for high heat input to the weld, ductile fracture mode of the weld is expected.

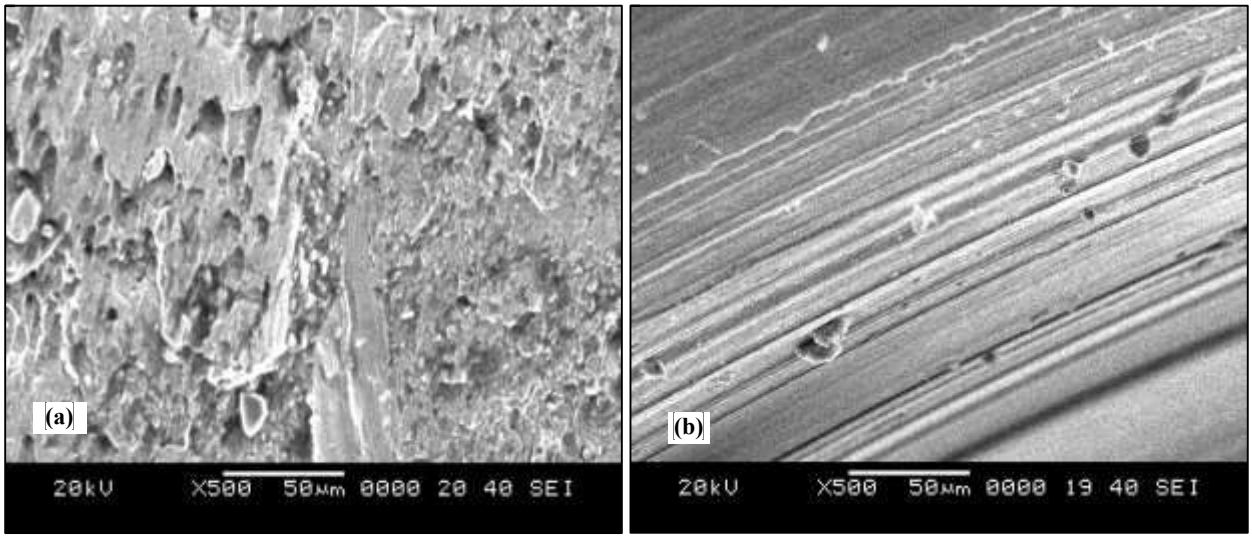

Figure 4.24: Fracture Surface Morphology (a) N=1200 rpm, V=20 mm/min, DT=2 seconds, (b) N=900 rpm, V=20, DT=2 seconds

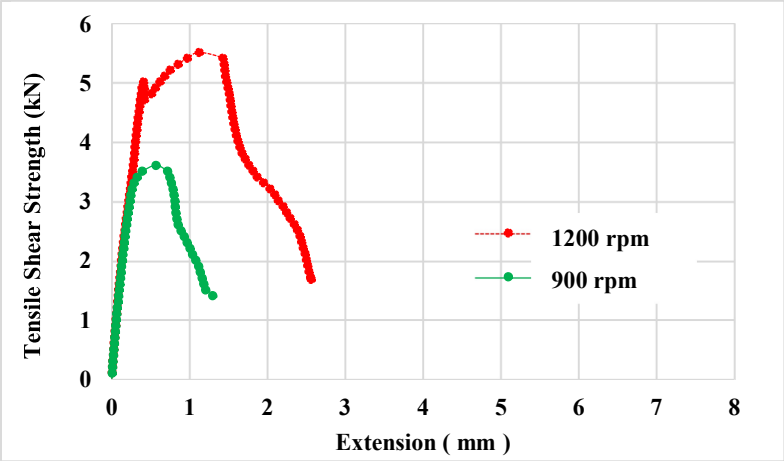

Figure 4.25: Tensile Shear Strength- Extension Graph, for V=20 mm/min and DT=2 seconds

4.5.3 Effect of Pin Tool Geometry on Fracture Surface Morphology

Welds that were produced using simple and threaded pin tool were compared in terms of fracture surface morphology. This has been performed using the analysis of fractured surface of the tensile shear strength failed samples.

Regular dimples were observed very close to the keyhole as shown in figure 4.26a on the fracture surface of FSSW welds performed using threaded pin tool at 900 rpm rotational speed, 20 mm/min plunging rate and 2 seconds dwell time. The presence of regular dimples indicates ductile fracture mode. This was found in agreement with references [39], [48], [31] and [61].

Figure 4.27 shows tensile shear strength extension plot for threaded and simple pin tools. Maximum extension using threaded pin tool of almost 7 mm was observed compared to 1.25 maximum extension for the welds performed using simple pin tool. This indicates ductile failure mode for welds of threaded pin tool. No dimples were observed in welds

that were performed using simple pin tool at 900 rpm, 20 mm/min and 2 seconds as shown in Figure 4.26b. Furthermore, fracture mode analysis based on photographs taken from failed samples after tensile shear strength test is conducted.

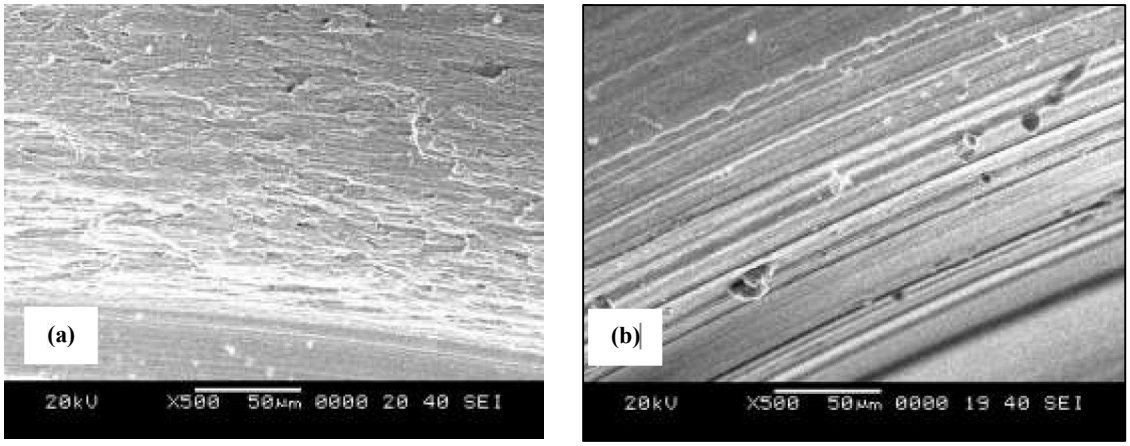

Figure 4.26: Fracture Surface Morphology (a) Threaded Pin Tool, (b) Simple Pin Tool

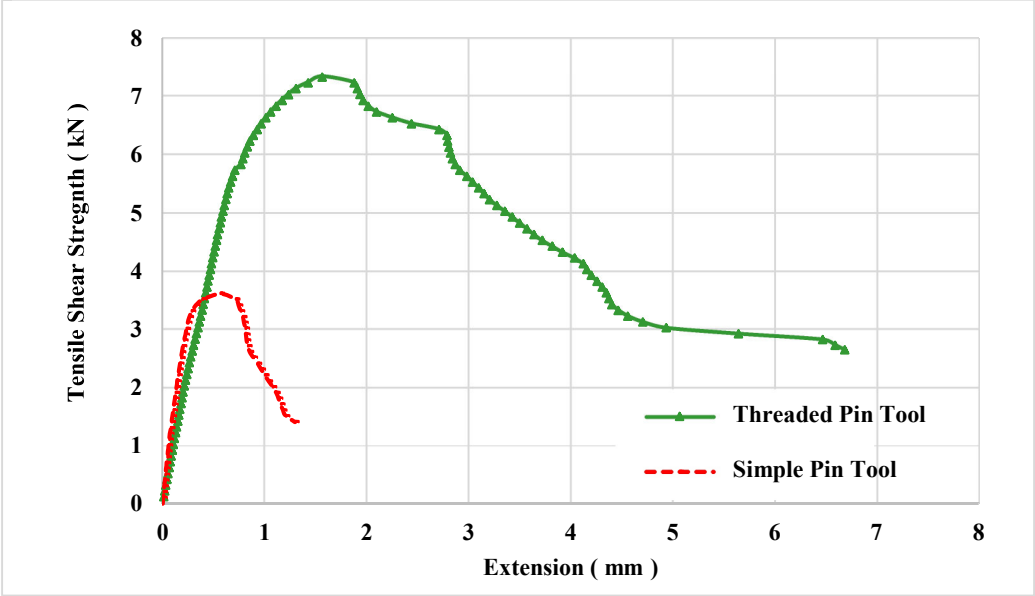

Figure 4.27: Tensile Shear Strength Extension Graph, for N=900 rpm, V=20 mm/min and DT=2 seconds

Two fracture modes were observed. Shear fracture mode as shown in Figure 4.28a to Figure 4.28c shows that the failure mechanism of fracture failure mode has occured. All welds were performed using simple pin tool. In shear fracture mode, the shear initiated from the hook (end of transition region), then propagates horizontally along the stir zone until the weld sheared off. This type of failure also called interfacial fracture or nugget fracture.

Pull out fracture mode called plug failure mode is reported by [31] and [35]. It was observed for threaded pin tool FSSW at 900 rpm, 20 mm/min and 2 and 4 seconds dwell time. In pull out fracture mode, the crack initiates from the transition region (interface of TMAZ and HAZ), then it propagates vertically along upper sheet thickness and finally pull out the nugget at final fracture phase. Pull out fracture mode is shown in Figure 4.29a and Figure 4.29b. Figure 4.29c shows pull out fracture mode failure mechanism.

Another explanation for the presence of dimple like surface morphology was highlighted by Venukumar *et al.* [25] and Tozaki *et al.* [62], in their experimental investigations of FSSW of aluminum alloys. They pointed out that the presence of extensive dimples in fracture surface of FSSW welds indicate strong lap joint bonding and high tensile shear strength. They found that all dimples like surface morphology welds showed high weld strength.

(a) (b) (c)

Figure 4.28: Shear Fracure Mode (a) Bottom View of The Upper Sheet, (b) Top View of the Lower Sheet, and (c) Shear Fracture Mechanism

(a) (b) (c)

Figure 4.29: Nugget Pull Out Fracture Mode (a) Top View (b) Bottom View of The Upper Sheet, (c) Pull Out Fracture Mechanism

Chapter 5

NUMERICAL MODELING OF FSSW PROCESS

5.1 Governing Equations

The governing equations that govern the thermo-mechanical model of friction stir spot welding process are as follows:

- Continuity equation is given in reference [63] as:

— (5.1)

: is the plastic flow velocity in x, y, z directions, and stands for partial differentiation.

- Momentum equation is given in reference [31] as:

——— — — □ — —□ — (5.2)

where ρ is the density of the work-piece, is the plastic flow velocity in x, y, z directions. The quantity is the pressure, is the velocity, and is the kinematic viscosity.

- Transient heat transfer governing equation is given in reference [30] as:

— (5.3)

where is the specific heat capacity, *k* is the thermal conductivity, *q* is the heat generated from friction deformation, *T* is the temperature, *t* is the time, is the divergence and is the gradient of a function and is defined by:

— — — (5.4)

5.2 Computational Techniques

Abaqus/Explicit offers three analysis methods. The suitable method for analysis is based on the physics of the problem according to reference [64].

5.2.1 Lagrangian Analysis

In Lagrangian analysis there is no flow of material. Material motion is restricted with the mesh. Material move with the deformation of the mesh. This analysis is appropriate for structural analysis. The limitation of Lagrangain model is the model termination due to excessive element distortion when severe deformation is experienced [64].

5.2.2 Eulerian Analysis

Eulerian analysis is suitable for problems involving severe deformation. In Eulerian analysis, nodes and mesh are fixed and the material is allowed to flow through the elements. The limitation of Eulerian analysis is that material deformation cannot be modeled as reported in reference [64].

5.2.3 Arbitrary Lagrangian Eulerian Analysis

In Arbitrary Lagrangian Eulerian (ALE) analysis, mesh is allowed to move and adapt itself during deformation. Limitation of this technique is that it cannot maintain high quality mesh in extreme distortion problems as reported in reference [64].

5.2.4 Coupled Eulerian-Lagrangian Analysis

In Coupled Eulerian Lagrangian (CEL) analysis, Abaqus allows to have two subdomains Eulerian and Lagrangian. CEL is the effective option when interaction of Lagrangian and Eulerian domains are needed. An example in finite element model of friction stir spot welding, pin tool and anvil are Lagrangian domains while work-piece where material flow is needed is Eulerian domain as reported in reference [64].

5.3 FE Modeling of FSSW

In this study the Coupled Eulerian Lagrangian (CEL) finite element model is developed using Abaqus® 6.13. In the CEL model, the tool is defined as a rigid Lagrangian body, while the work-piece is defined as Eulerian domain. This technique can provide a good prediction of material flow during the process as reported by Grujicic *et al.* [23]. The finite element model developed by Al-Badour [65] for FSW is adopted and refined in this study for FSSW.

5.3.1 Computational Domain

In the finite element model, both threaded pin, and scrolled shoulder were treated as a simple cylindrical pin and flat shoulder, respectively. For the work-piece, the area of interest taken into account, to minimize the number of elements, and enhance computational time was □□* □□mm^2. The work-piece geometry was partitioned into three zones, identifying the upper and lower plate and top layer of void. The layer of void (volume fraction was set equal to zero) was defined to allow the extruded material during the process to flow in this volume.

Void layer was used to allow the flash to develop during the process on the top surface of the upper plate. Void is defined in Abaqus® by assigning zero value to volume fraction value in material assignment. Figure 5.1 and 5.2 show the dimensions of the tool and the work-piece, respectively.

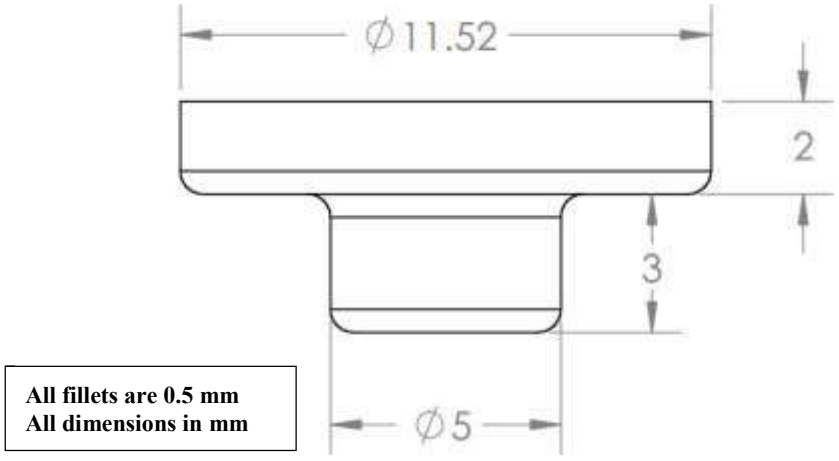

Figure 5.1: FSSW Tool Geometric Model Dimensions

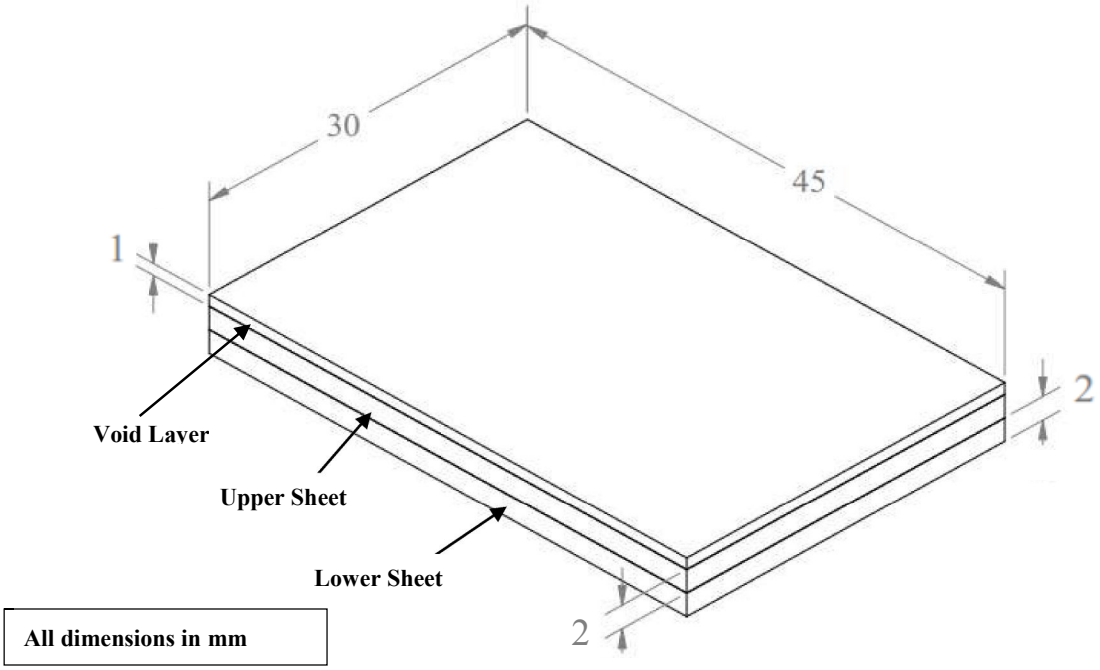

5.2: Geometric Model Dimensions of the Work-Piece

5.3.2 Finite Element Model Assumption

The following assumptions were considered in modeling the FSSW developed in this study.

- Linear elastic isotropic pin tool material is assumed.
- Film convection heat transfer coefficient on the top surface is 25 $W/m^2.k$ according to references [27] and [20].
- Thermal gap conductance on the bottom surface of the lower plate is 200 $W/m^2.k$.
- Lagrangian domain, rigid pin tool (because our interest is in temperature distribution, plastic strain distribution and work-piece material flow).
- Eulerian work- piece domain.
- Simple cylindrical pin tool.
- Flat pin tool shoulder to simplify Eulerian and Lagrangian domains discretization.
- Johnson-Cook material model.
- 90% of plastic deformation dissipated in the form of heat according to reference [66].
- Temperature dependent work-piece material properties.

5.3.3 Finite Element Meshing

Figure 5.3 shows structural hexahedral mesh for the pin tool having 1080 elements. Element Type used is linear hexahedral type C3D8RT. Bias seeding was used to achieve a refined mesh at the center of the work-piece and a coarse mesh at the sides. The work-piece was meshed with 79134 elements using an element type of EC3D8RT hexahedral linear thermally coupled Eulerian elements, as shown in Figure 5.4.

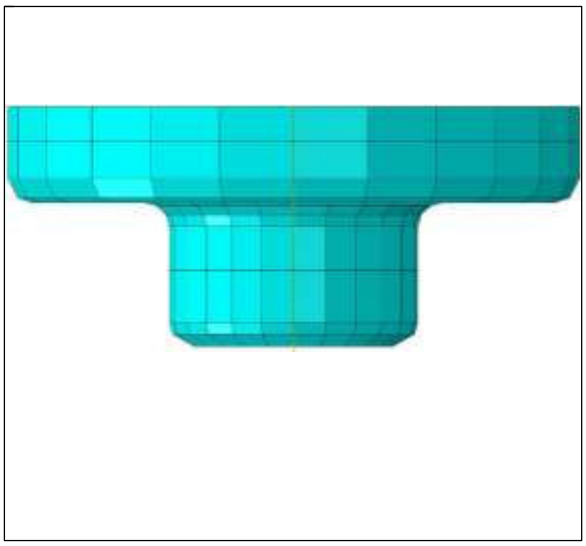

Figure 5.3: FSSW Pin Tool Mesh

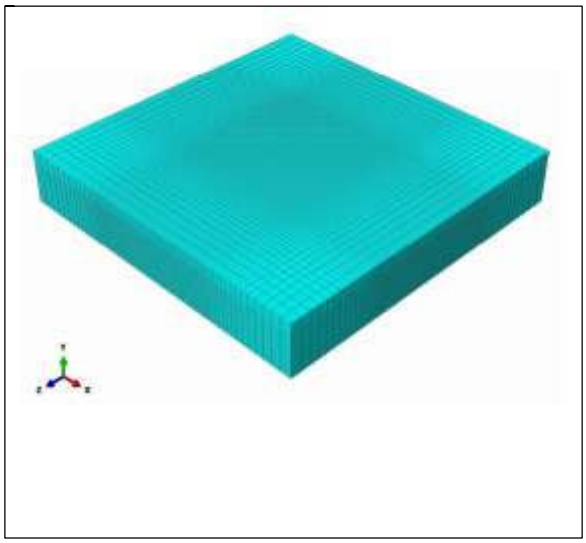

Figure 5.4: Work-Piece Mesh

5.3.4 Initial Conditions

Initial thermal and boundary conditions are mentioned for the adopted finite element model.

- Initial temperature is the ambient temperature 294.3 k (according to the thermocouple measurement).
- Constant pin tool rotational speed is assumed with zero initial translational speed.

- Void layer was assigned as a layer with 1 mm thickness on the whole overlapping area over the top surface of the upper sheet.
- Pure copper work-piece material was assigned in parallelepiped geometry with dimensions of □* □□* □□ mm3.

5.3.5 Boundary Conditions

Several boundary conditions were assumed in pre-processing of the finite element model. These boundary conditions are as follows:

- Gap heat conductance was assumed to be 200 $W/m^2.k$, to accommodate heat dissipation to the backing plate.
- Zero normal velocity on the bottom surface of the lower plate, is assumed to prevent the material from escape downward because it constrained by the backing plate.
- Material velocity at edges and bottom surface is zero, while it is allowed to flow at void zone.

5.3.6 Material Modeling

Since we have two computational domains, material was assigned for Lagrangian pin tool and Eulerian work-piece according to the following:

Work-Piece Material Modeling

Temperature dependent material properties such as thermal conductivity, elongation, elastic modulus and specific heat were defined for commercial pure Copper work-piece as given by Davis [67].

Johnson-Cook plastic stress flow model [68] was used to define the behavior of the material. Johnson-Cook [68] developed an experimental relationship that describes the influences of temperature, strain and strain rate on Von Mises stress. This relationship is expressed by [64] and [68], as

$$\text{Ц}w\cdot\square!\ W''\ И\acute{}\square\square\square W\#\ddot{}\text{Æ}\frac{\delta\dot{y}}{\delta_{\text{л}}}\square\square\square w\ \square 4^{\text{ц}}\square\ ] \qquad (5.5)$$

where Ц is the static stress, $И$ is the effective plastic strain, $И\dot{}$ is the current strain rate, $И_{\text{t}}$ is the reference strain rate. In the above equation, $\text{ъ}^{\text{ц}}$ is the homologous temperature and is defined by [64]

$$\text{ъ}^{\text{ц}}\ w\cdot\frac{\text{ъ}\ w\ \text{ъ}_{\text{ї}}}{\text{ъ}_{\text{ф}}\ w\ \text{ъ}_{\text{ї}}} \qquad (5.6)$$

where T_r is the room temperature, and T_m is the melting temperature. The constants A, B, C, n, m are given by Johnson-Cook [68]. Pure Copper Johnson Cook model constants are illustrated in Table 5.1.

Table 5.1 Pure Copper Johnson-Cook Constitutive Model Constants [68]

A [MPa]	B [MPa]	C	n	m	Melting Temp. [k]	Transition Temp. [k]
90	292	0.025	0.31	1.09	1356	298

Elongation, specific heat, elastic modulus and thermal expansion were defined as temperature dependent variables [67] to model the effect of temperature on material properties. Copper density was taken from reference [69] as 8940 kg/m^3. The FE model was implemented and solved using the Finite Element Analysis Abaqus® software package, in conjunction with thermally coupled explicit solver.

Tool Material Modeling

The tool was defined as rigid body. The tool material was modeled as linear-elastic carbon steel material, with a density of 7800 kg/m^3 according to reference [70]. The modulus of elasticity was taken as 200 GPa, thermal conductivity of 32 W/m.k and specific heat of 460 kJ/kg according to reference [65].

Time scaling factor of 1000 was used to accelerate the solution in Abaqus/Explicit analysis [64].

5.3.7 Tool / Work-piece Interaction Modeling

For the pin tool and work-piece interaction modeling the following assumptions were considered:

- Friction coefficient assumed to be 0.30 according to reference [71].
- Convection heat transfer in the upper plate is 25 W/m^2.k as reported in references [27] and [20].
- Thermal gap heat conductance is taken to be 200 w/m^2.k for the bottom surface of the lower plate. This value was assumed to be double the value that was considered by Wang *et al.* [72] for Aluminum alloy, since pure copper has double thermal conductivity of Aluminum.

5.4 FE Model Validation

Finite element model validation was carried out by considering two aspects of temperature distribution and material flow validation that will be discussed in what follows.

5.4.1 Temperature Distribution Validation

A K-type thermocouple was inserted 8.0 mm away from the weld center. The wire fitted to 0.5 mm machined hole was 1 mm depth. Figure 5.5 shows validation experiment setup.

Predicted temperatures were validated by comparing them with measured ones during FSSW at 8 mm from the weld center and 1 mm depth using K-type thermocouple. Figure 5.6 shows comparison between experimental and FE predictions at 600 rpm rotational speed for a sample having dimensions of □□□* □□* □ mm^3. The estimated temperatures are almost matching with the experimentally recorded ones, with a maximum difference of 16%.

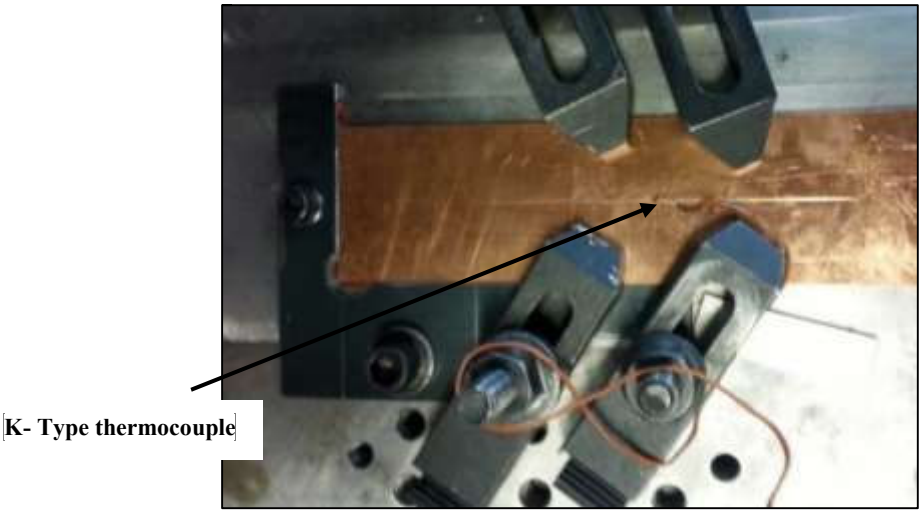

Figure 5.5: FE Validation Experiment Setup

Figures 5.6 to 5.8 show temperature variation at different welding parameters. Figure 5.6 shows comparison of FE model and experimental work temperature variation. According to the Figure experimental and FE model results match well to each other. Figure 5.7

shows temperature variation at 1200 rpm rotational speed, 60 mm/min plunging rate and 2 seconds dwell time. The temperature increase gradually during plunging phase (up to the third second) then sharp increase was observed at the end of plunging phase when the shoulder gets in contact with the work-piece because the shoulder produce most of frictional heat that is produced in FSSW process.

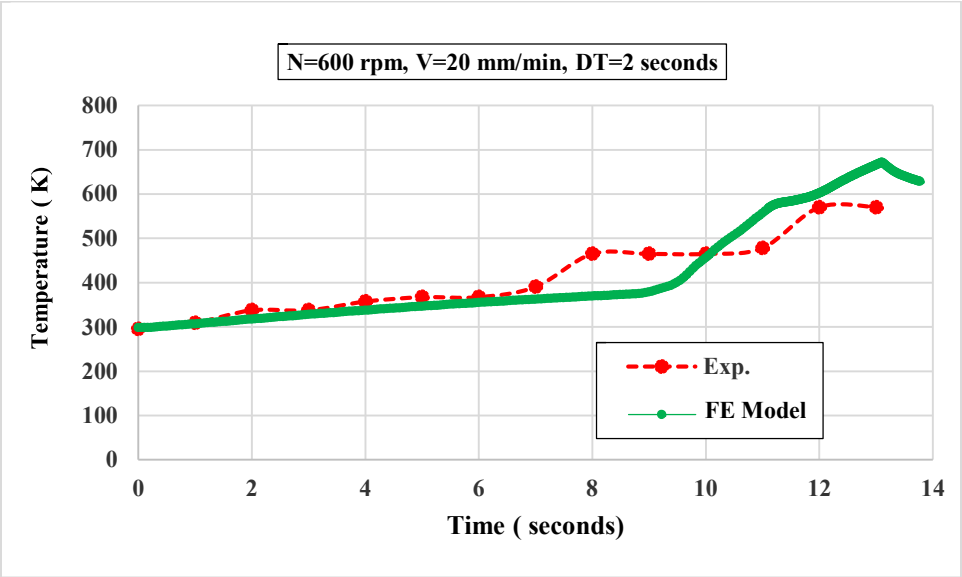

Figure 5.6: Temperature Variation at 8 mm Away From Weld Center 1 mm Depth, 100X30X2 mm^3 Samples

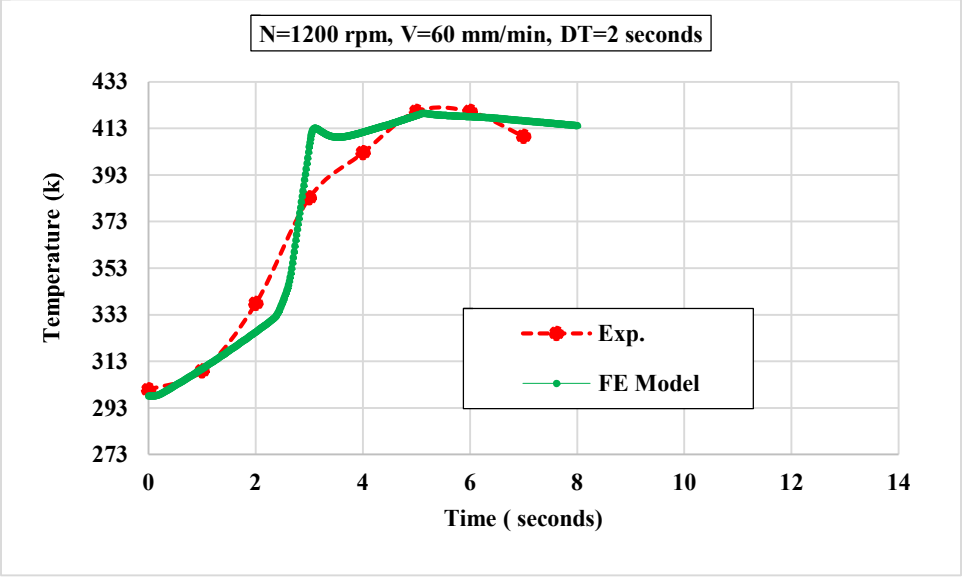

Figure 5.7: Temperature Variation at 9.5 mm Away from Weld Center 2 mm Depth, 138X60X2 mm^3 Samples

Figure 5.8 shows temperature distribution at 1200 rpm rotational speed, 20 mm/min plunging rate and 2 seconds dwell time. The temperature increases gradually with time during plunging phase up to the ninth second. After that, the temperature increases rapidly according to finite element model and experimental temperature history. This rapid increase in temperature at the end of plunging phase when the shoulder touches the work-piece indicates the dominant effect of the shoulder frictional heat on the heat input to the weld.

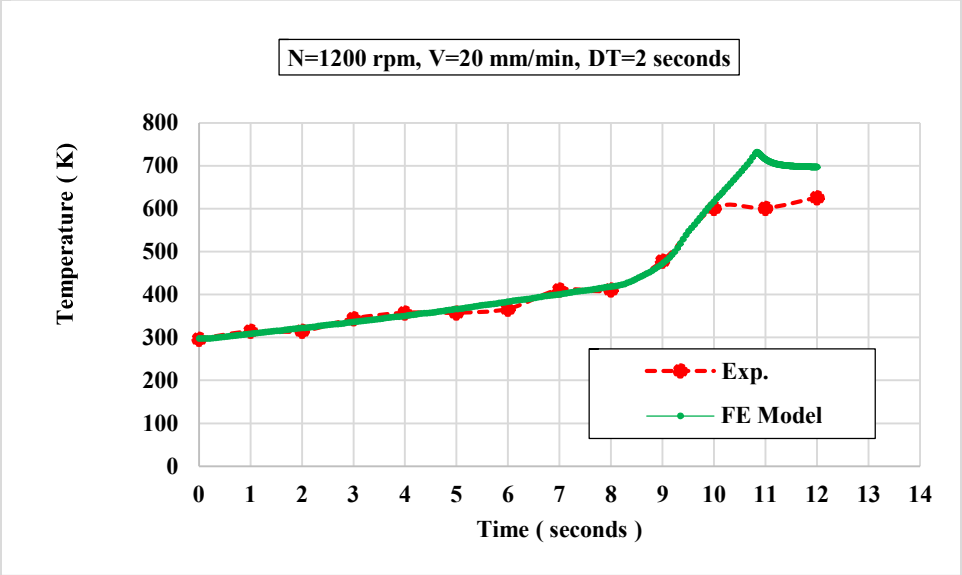

Figure 5.8: Temperature Variation at 9.5 mm Away from Weld Center 2 mm Depth 138X60X2 mm^3 Samples.

5.4.2 Extruded Flash Height Validation

Figure 5.9 shows the finite element model for the predicted flash height compared to the experimental one. The developed experimental flash height was 0.6 mm while the height of flash from finite element model after pin tool retraction was 0.64 mm.. However, a good agreement between welds flash height and predicted flash height was obtained with an error of 6.6%.

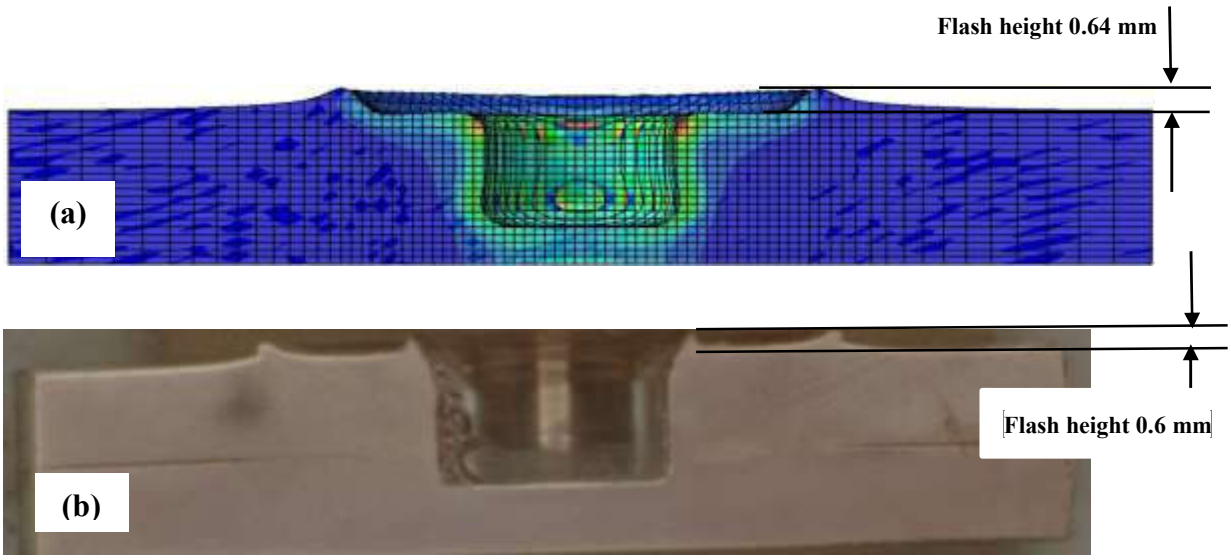

Figure 5.9: Material Flow Validation (a) Finite Element Results, (b) Optical Macrograph of FSSW Weld Cross-Section at N=1200 rpm, V=20 mm/min and DT=2 seconds Using Simple Pin Tool

5.5 FE Model Results

Effect of welding parameters on temperature distribution and plastic strain distribution at the end of dwell time is presented in this section.

5.5.1 Temperature Distribution Analysis

The following contour plots show the temperature distributions at the end of dwell time. Increase of dwell time from 2 to 4 seconds, as shown in Figure 5.10, increased the peak temperature experienced by the work-piece from 750 k to 820 k at 900 rpm rotational speed and 20 mm/min plunging rate. Increase of rotational speed from 900 to 1200 rpm increased the peak temperature from 750 k to 850 k as shown in Figure 5.10a and 5.12a. On the other hand, increase of plunging rate from 20 to 60 mm/min decrease the peak temperature from 750 k to 614 k as shown in Figure 5.10a and 5.11a, respectively.

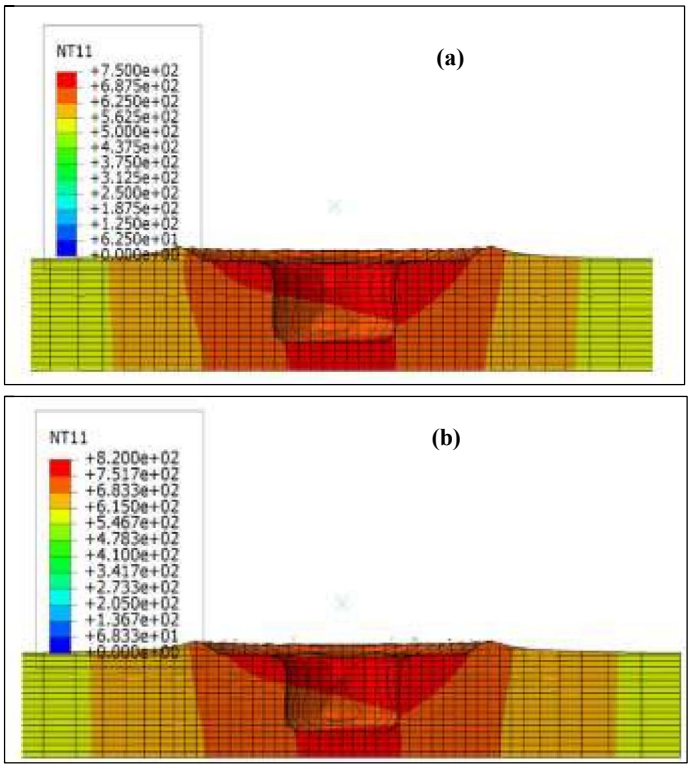

Figure 5.10: Temperature Distribution at End of Dwell Time (a) N=900 rpm, V= 20 mm/min, DT=2 seconds, (b) N=900 rpm, V= 20 mm/min, DT=4 seconds

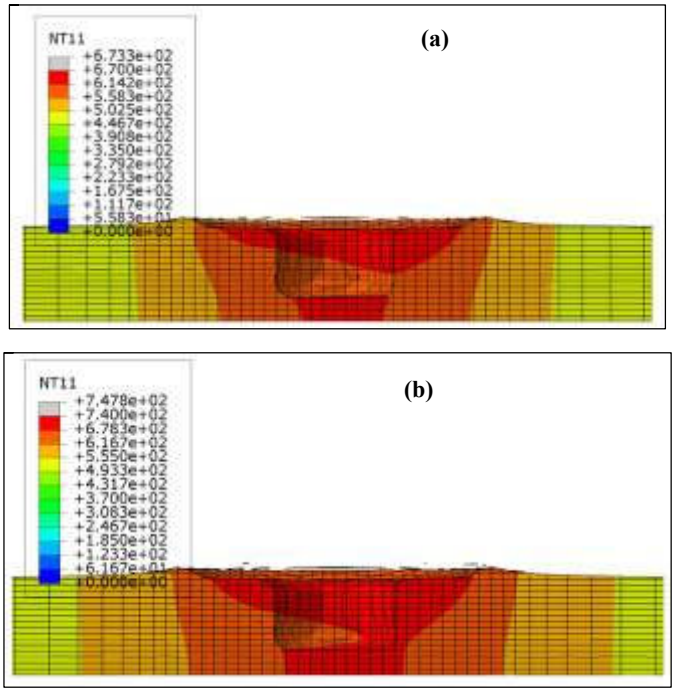

Figure 5.11: Temperature Distribution at End of Dwell Time, (a) N=900 rpm, V= 60 mm/min, DT=2 second, (b) N=900 rpm, V= 60 mm/min, DT=4 seconds

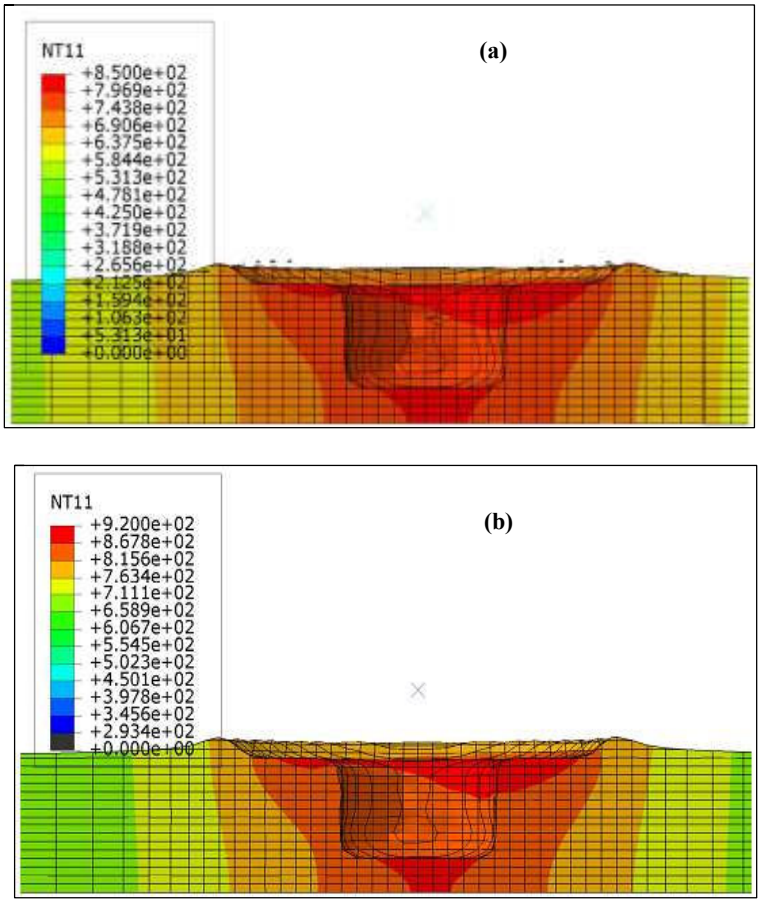

Figure 5.12: Temperature Distribution at End of Dwell Time, (a) N=1200 rpm, V= 20 mm/min, DT=2 second, (b) N=1200 rpm, V= 20 mm/min, DT=4 second

Increasing of dwell time from 2 to 4 seconds at 1200 rpm, 60 mm/min plunging rate, increases the peak temperature from 715 k to 860 k as shown in figure 5.13a and 5.13b respectively.

Increasing of the dwell time from 2 to 4 seconds at 900 rpm, 60 mm/min plunging rate, increases the peak temperature of the work-piece from 670 k to 740 k.

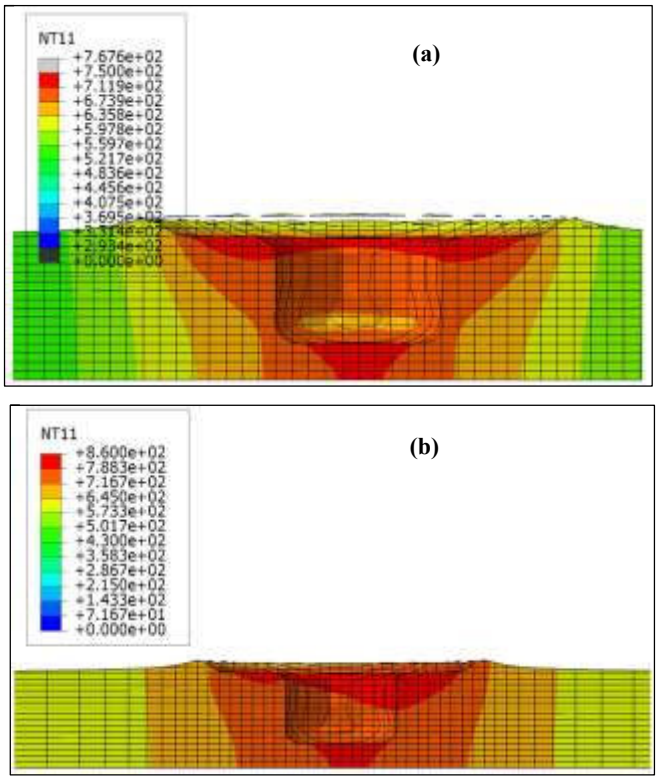

Figure 5.13: Temperature Distribution at End of Dwell Time, (a) N=1200 rpm, V= 60 mm/min, DT=2 seconds, (b) N=1200 rpm, V= 60 mm/min, DT=4 seconds

The peak temperature for each set of welding parameters was determined and full factorial design of experiment is carried out in the following section.

5.5.2 Full Factorial Design of Experiment for Peak Temperature

The FE model was used to carry out a virtual design of experiment. The entries of the experimental matrix were introduced into the model by changing boundary conditions accordingly.

Figure 5.14 shows the main effect of welding parameters on peak temperature during FSSW. Varying rotational speed from 900 to 1200 rpm increases the peak temperature reached during the process at the end of dwell time.

Increasing the dwell time from 2 seconds to 4 seconds and increasing rotational speed from 900 to 1200 rpm, resulted in increase of peak temperature. Increasing of plunging rate decreases peak temperature as shown in figure 5.15.

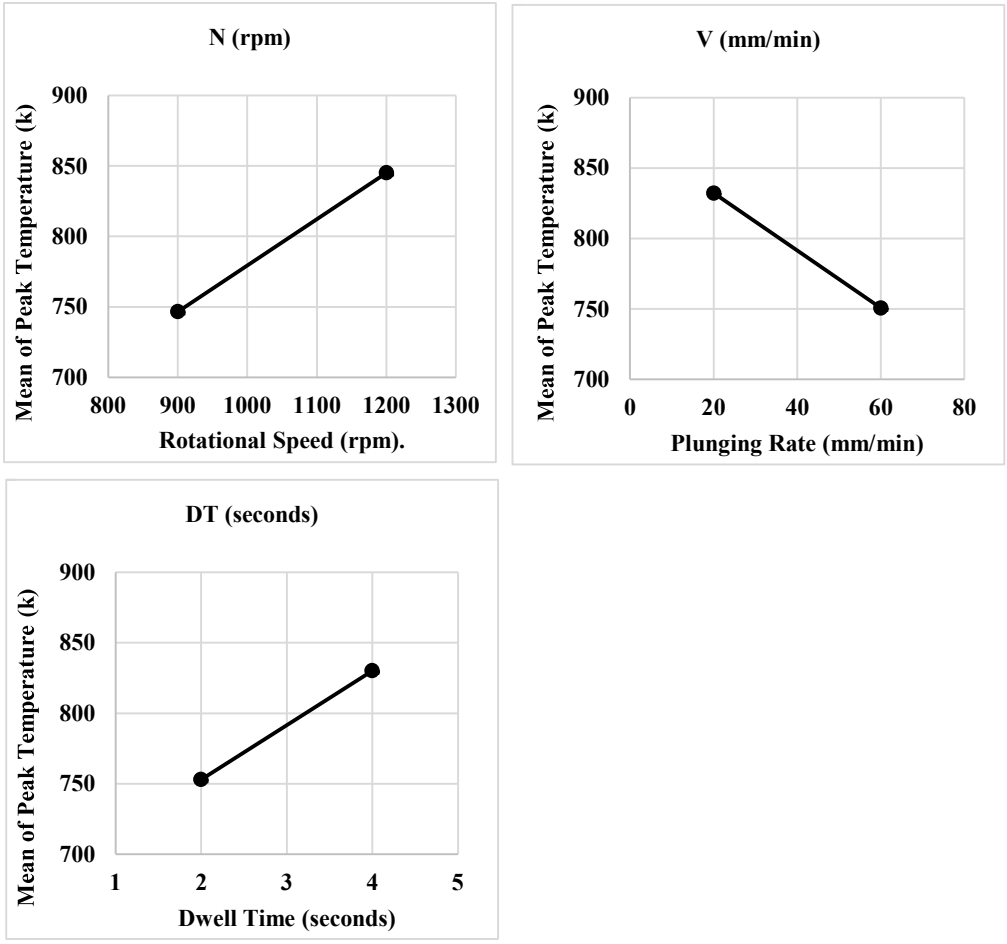

Figure 5.14: Main Effect Plot of FE Model Peak Temperatures at End of Dwell Time

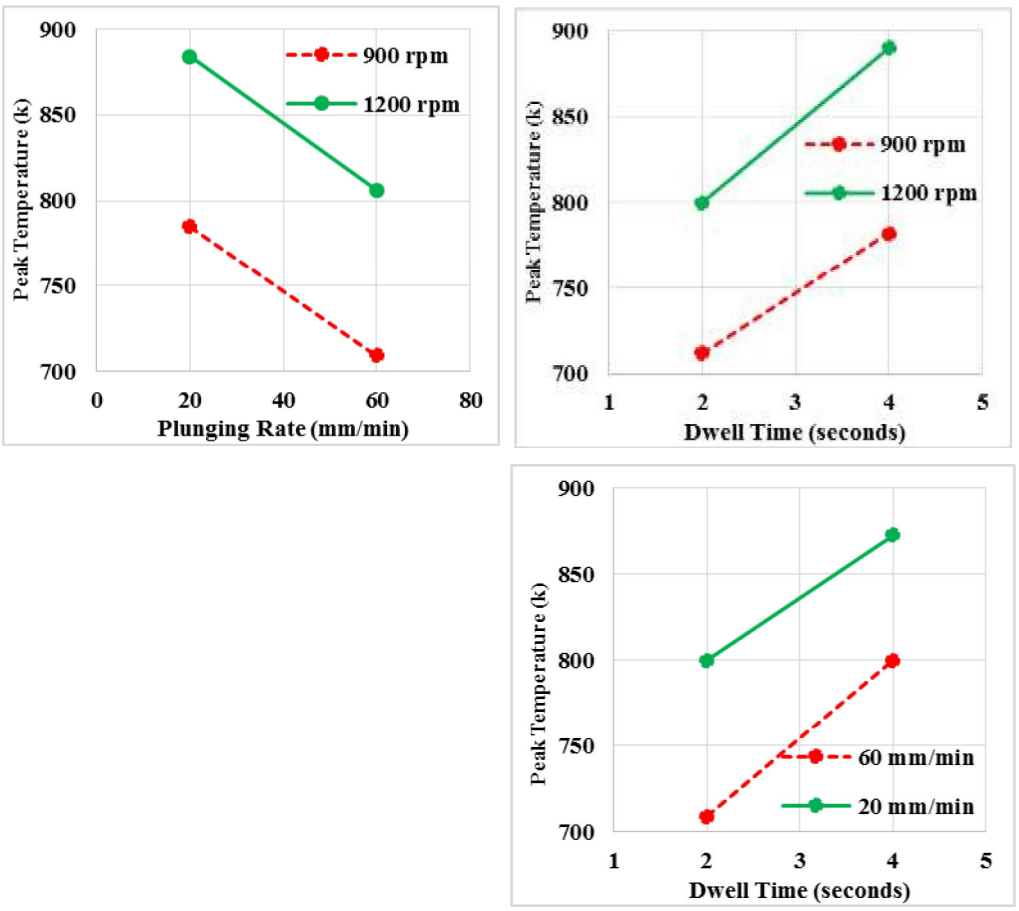

Figure 5.15: Interaction Effect Plot of FE Model Peak Temperature at End of Dwell Time

Analysis of Variance (ANOVA) illustrated in Table 5.2 shows that the rotational speed has the most significant process parameter effect on peak temperature because it has the least P-value.

Table 5.2 P-Values from Analysis of Variance of DoE Parameters of Max Temp Output

Welding Parameters	P: Probability Distribution
Rotational Speed N [rpm]	0.001
Plunging Rate V [mm/min]	0.002
Dwell Time DT [seconds]	0.002

Chapter 6

CONCLUSIONS AND FUTURE WORK

6.1 Conclusions

In this investigation, an experimental as well as numerical study of FSSW of a pure copper lap joint were carried out at different process parameters including rotational speed, plunging rate and dwell time. Two pin tools were used, a simple pin tool and a threaded one. The threaded pin tool was used to compare its performance with the simple one. Weld joint quality was characterized using different techniques namely scanning electron microscopy, optical microscope and micro-hardness tester. Furthermore, finite element model is developed to assist in the understanding of the process.

From the current forging force analysis results, it can be concluded that increasing of the plunging rate and decreasing of rotational speed and dwell time correspond to increase in maximum forging force due to lower heat input and material plasticization for the simple pin tool.

The effect of FSSW process parameters on hook formation was analyzed using high magnification micrographs. The following conclusions can be made:

- Varying of dwell time from 2 to 4 seconds resulted in more white bubbles in hook feature at 1200 rpm rotational speed, and 20 mm/min plunging rate. These white bubbles were observed at high heat input to the weld.

- Smooth hook feature, free of voids, cracks and discontinuities were observed at 1200 rpm rotational speed, 20 mm/min plunging rate and 2 seconds dwell time. Highest tensile shear strength to the weld was obtained at the same welding conditions using simple pin tool.
- Cracks, voids and discontinuities were observed at 1200 rpm rotational speed, 60 mm/min plunging rate and 2 seconds dwell time. Low weld tensile shear strength was obtained at these welding conditions using a simple pin tool.

The effect of process parameters on effective upper sheet thickness has been studied, for effective upper sheet analysis. The following conclusions can be made:

- Downward inclination indicates low material flow during the process resulted in lower weld tensile shear strength.
- Upward hook tip inclination was observed in threaded pin tool welds for 20 mm/min plunging rate. This corresponds to relatively high tensile shear strength and enhanced material flow during the process.

For the effect of FSSW process parameters on tensile shear strength, the following conclusions can be highlighted from design of experiments results:

- ANOVA analysis of tensile shear strength experimental results showed that rotational speed has the most significant effect on tensile shear strength.
- Maximum tensile shear strength of 5.5 kN was obtained for a simple pin tool was used at 1200 rpm rotational speed, 20 mm/min plunging rate and 2 seconds dwell time.

- Tensile shear strength of 7.1 kN, was obtained at 900 rpm rotational speed, 20 mm/min plunging rate, 2 seconds dwell time using threaded pin tool. A simple pin tool produced 3.5 kN tensile shear strength at the same welding conditions (i.e. an increase of 50 % in weld strength).

Fracture surface morphology has been investigated in this work. From the current results, it can be concluded that:

- Dimple like surface morphology was observed using threaded pin tool at 1200 rpm rotational speed, 20 mm/min plunging rate and 2 seconds dwell time with ductile failure mode at these welding conditions.
- Plug or pull out fracture mode was observed at 900 rpm – 20 mm/min – 2 seconds for threaded pin tool and 1200 rpm rotational speed, 20 mm/min plunging rate and 2 and 4 seconds dwell times for simple pin tool.

Lastly finite element model has been developed in this study to find the effect of welding parameters on temperature distribution. The following conclusions can be drawn:

- Experimental temperature history was compared with predicted finite element model temperature at the same location that is 8 mm from weld center with 2 mm depth. Predicted temperature matched well with temperature history from the experiment with maximum error of 16%.

- Flash height of weld cross-section and predicted flash height from the model were compared. A maximum error of 6.6% was found.
- ANOVA analysis revealed that rotational speed has the most significant effect on peak temperature.
- Increasing of dwell time and decreasing of plunging rate resulted in increasing predicted peak temperature of the workpiece.

6.2 Future Work

- High thermal resistance pin tool material could allow the analysis of 1500 rpm rotational speed to the weld.
- Tracer particles could be introduced to the finite element model developed in this work to study the effect of welding parameters on material flow during welding.
- Analysis of Copper alloys and Copper to Copper alloys dissimilar friction stir spot welding using initially the welding parameters carried out in this investigation. Copper alloys have many application in heat exchangers.
- Tracer particles could be introduced to the finite element model developed in current study for material flow analysis.

References

[1] Y. F. Sun, H. Fujii, N. Takaki, and Y. Okitsu, "Microstructure and Mechanical Properties of Mild Steel Joints Prepared by a Flat Friction Stir Spot Welding Technique", *Mater. Des.*, vol. 37, pp. 384–392, 2012.

[2] W. Yuan, R. S. Mishra, S. Webb, Y. L. Chen, B. Carlson, D. R. Herling, and G. J. Grant, "Effect of Tool Design and Process Parameters on Properties of Al Alloy 6016 Friction Stir Spot Welds", *J. Mater. Process. Technol.*, vol. 211, no. 6, pp. 972–977, June 2011.

[3] R. S. Mishra and Z. Y. Ma, "Friction Stir Welding and Processing", *Mater. Sci. Eng. R Reports*, vol. 50, no. 1, pp. 1–78, Aug. 2005.

[4] http://www.teknomega.com/image/image_gallery_uuid=239f3b2b-4da8-4775-9cfe-2fe1a76e404d&groupId=107550&t=1291823035117, accessed on 18/4/2015.

[5] D. H. Choi, B. W. Ahn, C. Y. Lee, Y. M. Yeon, K. Song, and S. B. Jung, "Formation of Intermetallic Compounds in Al and Mg Alloy Interface During Friction Stir Spot Welding", *Intermetallics*, vol. 19, no. 2, pp. 125–130, Feb. 2011.

[6] W. Yuan, R. S. Mishra, B. Carlson, R. Verma, and R. K. Mishra, "Material Flow and Microstructural Evolution During Friction Stir Spot Welding of AZ31 Magnesium Alloy", *Mater. Sci. Eng. A*, vol. 543, pp. 200–209, May 2012.

[7] A. Gerlich, G. Avramovic Cingara, and T. H. North, "Stir Zone Microstructure and Strain Rate During Al 7075-T6 Friction Stir Spot Welding", *Metall. Mater. Trans. A*, vol. 37, no. 9, pp. 2773–2786, Sep. 2006.

[8] S. Hirasawa, H. Badarinarayan, K. Okamoto, T. Tomimura, and T. Kawanami, "Analysis of Effect of Tool Geometry on Plastic Flow During Friction Stir Spot Welding Using Particle Method", *J. Mater. Process. Technol.*, vol. 210, no. 11, pp. 1455–1463, 2010.

[9] H. S. Shin, "Tool Geometry Effect on the Characteristics of Dissimilar Friction Stir Spot Welded Bulk Metallic Glass to Lightweight Alloys", *J. Alloys Compd.*, vol. 586, pp. S50–S55, Feb. 2014.

[10] H. M. Rao, R. I. Rodriguez, J. B. Jordon, M. E. Barkey, Y. B. Guo, H. Badarinarayan, and W. Yuan, "Friction Stir Spot Welding of Rare-Earth Containing ZEK100 Magnesium Alloy Sheets", *Mater. Des.*, vol. 56, pp. 750-754, 2013.

[11] H. Badarinarayan, Y. Shi, X. Li, and K. Okamoto, "Effect of Tool Geometry on Hook Formation and Static Strength of Friction Stir Spot Welded Aluminum 5754-O Sheets", *Int. J. Mach. Tools Manuf.*, vol. 49, no. 11, pp. 814–823, Sep. 2009.

[12] M. Merzoug, M. Mazari, L. Berrahal, and A. Imad, "Parametric studies of the Process Of Friction Spot Stir Welding of Aluminium 6060-T5 Alloys", *Mater. Des.*, vol. 31, no. 6, pp. 3023–3028, June 2010.

[13] Kulekci, M. K., Esme, U., & Er, O., (2011), "Experimental Comparison of Resistance Spot Welding and Friction-Stir Spot Welding Processes for the EN AW 5005 Aluminum Alloy", *Journal of Material and Technology*, vol. 45, no. 5, pp. 395–399, 2011.

[14] M. I. Khan, M. L. Kuntz, P. Su, A. Gerlich, T. North, and Y. Zhou, "Resistance and Friction Stir Spot Welding of DP600: A Comparative Study", *Sci. Technol. Weld. Join.*, vol. 12, no. 2, pp. 175–182, Feb. 2007.

[15] Q. Yang, S. Mironov, Y. S. Sato, and K. Okamoto, "Material Flow During Friction Stir Spot Welding", *Mater. Sci. Eng. A*, vol. 527, no. 16–17, pp. 4389–4398, June 2010.

[16] P. Su, A. Gerlich, T. H. North, and G. J. Bendzsak, "Intermixing in Dissimilar Friction Stir Spot Welds", *Metall. Mater. Trans. A*, vol. 38, no. 3, pp. 584–595, Mar. 2007.

[17] Y. F. Sun, J. M. Shen, Y. Morisada, and H. Fujii, "Spot Friction Stir Welding of Low Carbon Steel Plates Preheated by High Frequency Induction", *Mater. Des.*, vol. 54, pp. 450–457, 2014.

[18] S. Mandal, J. Rice, and A. A. Elmustafa, "Experimental and Numerical Investigation of the Plunge Stage in Friction Stir Welding", *J. Mater. Process. Technol.*, vol. 203, no. 1, pp. 411–419, Jul. 2008.

[19] M. Assidi, L. Fourment, S. Guerdoux, and T. Nelson, "Friction Model for Friction Stir Welding Process Simulation: Calibrations From Welding Experiments", *Int. J. Mach. Tools Manuf.*, vol. 50, no. 2, pp. 143–155, Feb. 2010.

[20] M. Reilly, "Modelling of Friction Stir Spot Welding", *Ph.D. Dissertation*, Unversity of Cambridge, UK., 2013.

[21] M. Awang, "Simulation of Friction Stir Spot Welding (FSSW) Process Study of Friction Phenomena", *Ph.D. Dissertation*, West Verginia University, USA, 2007.

[22] P. Su, A. Gerlich, T. H. North, and G. J. Bendzsak, "Energy Utilisation and Generation During Friction Stir Spot Welding", *Sci. Technol. Weld. Join.*, vol. 11, no. 2, pp. 163–169, 2006.

[23] M. Grujicic, G. Arakere, B. Pandurangan, J. M. Ochterbeck, C. F. Yen, B. A. Cheeseman, A. P. Reynolds, and M. A. Sutton, "Computational Analysis of Material Flow During Friction Stir Welding of AA5059 Aluminum Alloys", *J. Mater. Eng. Perform.*, vol. 21, no. 9, pp. 1824–1840, Oct. 2011.

[24] M. Grujicic, T. He, G. Arakere, H. V. Yalavarthy, C. F. Yen, and B. A. Cheeseman, "Fully Coupled Thermomechanical Finite Element Analysis of Material Evolution During Friction-Stir Welding of AA5083", *Proc. Inst. Mech. Eng. Part B J. Eng. Manuf.*, vol. 224, no. 4, pp. 609–625, 2010.

[25] S. Venukumar, S. Yalagi, and S. Muthukumaran, "Comparison of Microstructure and Mechanical Properties of Conventional and Refilled Friction Stir Spot Welds in AA 6061-T6 Using Filler Plate", *Trans. Nonferrous Met. Soc. China*, vol. 23, no. 10, pp. 2833–2842, Oct. 2013.

[26] Y. F. Sun, H. Fujii, N. Takaki, and Y. Okitsu, "Microstructure and Mechanical Properties of Dissimilar Al Alloy/Steel Joints Prepared by A Flat Spot Friction Stir Welding Technique", *Mater. Des.*, vol. 47, pp. 350–357, May 2013.

[27] K. H. Muci-Küchler, S. Kalagara, and W. J. Arbegast, "Simulation of a Refill Friction Stir Spot Welding Process Using a Fully Coupled Thermo-Mechanical FEM Model", *J. Manuf. Sci. Eng.*, vol. 132, no. 1, p. 014503-1-5, 2010.

[28] Z. Zhang, X. Wang, P. Wang, and G. Zhao, "Friction Stir Keyholeless Spot Welding of AZ31 Mg Alloy-Mild Steel", *Trans. Nonferrous Met. Soc. China*, vol. 24, no. 6, pp. 1709–1716, June 2014.

[29] Y. Tozaki, Y. Uematsu, and K. Tokaji, "Effect of Tool Geometry on Microstructure and Static Strength in Friction Stir Spot Welded Aluminium Alloys", *Int. J. Mach. Tools Manuf.*, vol. 47, no. 15, pp. 2230–2236, Dec. 2007.

[30] C. D. Cox, J. R. Aguilar, M. C. Ballun, A. M. Strauss, and G. E. Cook, "The Application of a Pinless Tool in Friction Stir Spot Welding: an Experimental and Numerical Study", *Proc. Inst. Mech. Eng. Part D J. Automob. Eng.*, vol. 228, no. 11, pp. 1359–1370, May 2014.

[31] Z. Shen, X. Yang, Z. Zhang, L. Cui, and T. Li, “Microstructure and Failure Mechanisms of Refill Friction Stir Spot Welded 7075-T6 Aluminum Alloy Joints”, *Mater. Des.*, vol. 44, pp. 476–486, 2013.

[32] A. Gerlich, M. Yamamoto, and T. H. North, “Local Melting and Tool Slippage During Friction Stir Spot Welding of Al-Alloys”, *J. Mater. Sci.*, vol. 43, no. 1, pp. 2–11, Nov. 2007.

[33] D. A. Wang and S. C. Lee, “Microstructures and Failure Mechanisms of Friction Stir Spot Welds of Aluminum 6061-T6 sheets”, *J. Mater. Process. Technol.*, vol. 186, no. 1, pp. 291–297, May 2007.

[34] D. A. Wang and C. H. Chen, “Fatigue Lives of Friction Stir Spot Welds in Aluminum 6061-T6 Sheets”, *J. Mater. Process. Technol.*, vol. 209, no. 1, pp. 367–375, Jan. 2009.

[35] Y. Uematsu, K. Tokaji, Y. Tozaki, T. Kurita, and S. Murata, “Effect of Re-Filling Probe Hole on Tensile Failure and Fatigue Behaviour of Friction Stir Spot Welded Joints in Al-Mg-Si Alloy”, *Int. J. Fatigue*, vol. 30, no. 10, pp. 1956–1966, Oct. 2008.

[36] D. Mitlin, V. Radmilovic, T. Pan, J. Chen, Z. Feng, and M. L. Santella, “Structure–Properties Relations in Spot Friction Welded (Also Known as Friction Stir Spot Welded) 6111 Aluminum”, *Mater. Sci. Eng. A*, vol. 441, no. 1, pp. 79–96, Dec. 2006.

[37] A. Kumar and L. S. Raju, “Influence of Tool Pin Profiles on Friction Stir Welding of Copper”, *Mater. Manuf. Process.*, vol. 27, no. 12, pp. 1414–1418, Dec. 2012.

[38] H. S. Park, T. Kimura, T. Murakami, Y. Nagano, K. Nakata, and M. Ushio, “Microstructures and Mechanical Properties of Friction Stir Welds of 60% Cu–40% Zn Copper Alloy”, *Mater. Sci. Eng. A*, vol. 371, no. 1, pp. 160–169, Apr. 2004.

[39] T. Sakthivel and J. Mukhopadhyay, “Microstructure and Mechanical Properties of Friction Stir Welded Copper”, *J. Mater. Sci.*, vol. 42, no. 19, pp. 8126–8129, June 2007.

[40] C. Meran and V. Kovan, “Microstructures and Mechanical Properties of Friction Stir Welded Dissimilar Copper/Brass Joints”, *Mat.-wiss. u. Werkstofftech.,* vol. 39, no. 8, pp. 521–530, 2008.

[41] L. Cederqvist, C. D. Sorensen, A. P. Reynolds, and T. Öberg, “Improved Process Stability During Friction Stir Welding of 5 cm Thick Copper Canisters Through

Shoulder Geometry and Parameter Studies", *Sci. Technol. Weld. Join.*, vol. 14, no. 2, pp. 178–184, Feb. 2009.

[42] C. G. Andersson, R. E. Andrews, Proceedings of the First International Symposium on Friction Stir Welding, Thousand Oaks, CA, USA, June 1999.

[43] C. G. Andersson, R.E. Andrews, B. G. I. Dance, M. J. Russell, E. J. Olden, R. M. Sanderson, Proceedings of the Second Symposium on Friction Stir Welding, Gothenburg, Sweden, June 2000.

[44] I. Galvão, R. M. Leal, D. M. Rodrigues, and A. Loureiro, "Influence of Tool Shoulder Geometry on Properties of Friction Stir Welds in Thin Copper Sheets", *J. Mater. Process. Technol.*, vol. 213, pp. 129–135, 2013.

[45] A. Heidarzadeh and T. Saeid, "Prediction of Mechanical Properties in Friction Stir Welds of Pure Copper", *Mater. Des.*, vol. 52, pp. 1077–1087, 2013.

[46] R. Heideman, C. Johnson, and S. Kou, "Metallurgical Analysis of Al/Cu Friction Stir Spot Welding", *Sci. Technol. Weld. Join.*, vol. 15, no. 7, pp. 597–604, 2010.

[47] W. B. Lee and S.-B. Jung, "The Joint Properties of Copper by Friction Stir Welding", *Mater. Lett.*, vol. 58, no. 6, pp. 1041–1046, Feb. 2004.

[48] N. Xu, R. Ueji, Y. Morisada, and H. Fujii, "Modification of Mechanical Properties of Friction Stir Welded Cu Joint by Additional Liquid CO_2 Cooling", *Mater. Des.*, vol. 56, pp. 20–25, 2014.

[49] R. Karthikeyan and V. Balasubramanian, "Predictions of the Optimized Friction Stir Spot Welding Process Parameters for Joining AA2024 Aluminum Alloy Using RSM", *Int. J. Adv. Manuf. Technol.*, vol. 51, no. 1, pp. 173–183, Apr. 2010.

[50] G. Fernandez and L. Murr, "Characterization of Tool Wear and Weld Optimization in The Friction-Stir Welding Of Cast Aluminum 359+20% SiC Metal-Matrix Composite", *Mater. Charact.*, vol. 52, no. 1, pp. 65–75, Mar. 2004.

[51] X. Cao and M. Jahazi, "Effect of Tool Rotational Speed and Probe Length on Lap Joint Quality of A Friction Stir Welded Magnesium Alloy", *Mater. Des.*, vol. 32, no. 1, pp. 1–11, Jan. 2011.

[52] A. K. Mahgoub, A. Bazoune, F. A. A. Al-Badour, A. Shuaib, and G. M. Karrar, "Experimental Study and Numerical Modeling of Friction Stir Spot Welding of Pure

Copper Lap Joint", in *ASME 2014 International Mechanical Engineering Congress and Exposition*, Montreal, Canada, Nov. 2014.

[53] Minitab®17 Statistical Software.

[54] ASTM-International Standard Test Methods for Tension Testing of Metallic Materials, E8M, 2009.

[55] Manufaturing Technology Incorporation (MTI), Scrolled Shoulder, Part No. MTI011791.

[56] AWS Standard D8-9 1997.

[57] A. N. Shuaib, N. Merah and A. Bazoune, "Developing A Friction Stir Welding Process for Joining Similar and Dissimilar Materials in Heat Transfer Equipment", NSTIP Project No-08-ADV66-04, 2014.

[58] Z. Zhang, X. Yang, J. Zhang, G. Zhou, X. Xu, and B. Zou, "Effect of Welding Parameters on Microstructure and Mechanical Properties of Friction Stir Spot Welded 5052 Aluminum Alloy", *Mater. Des.*, vol. 32, no. 8, pp. 4461–4470, Sep. 2011.

[59] Y. F. F. Sun, J. M. M. Shen, Y. Morisada, and H. Fujii, "Spot Friction Stir Welding of Low Carbon Steel Plates Preheated by High Frequency Induction", *Mater. Des.*, vol. 54, pp. 450–457, Feb. 2014.

[60] C. D. Cox, B. T. Gibson, A. M. Strauss, and G. E. Cook, "Effect of Pin Length and Rotation Rate on The Tensile Strength of A Friction Stir Spot-Welded Al Alloy: A Contribution to Automated Production", *Mater. Manuf. Process.*, vol. 27, no. 4, pp. 472–478, 2012.

[61] T. G. Nieh and W. D. Nix, "A Comparison of the Dimple Spacing on Intergranular Creep Fracture Surfaces With the Slip Band Spacing for Copper", *Scr. Metall.*, vol. 14, no. 3, pp. 365–368, 1980.

[62] Y. Tozaki, Y. Uematsu, and K. Tokaji, "A Newly Developed Tool Without Probe for Friction Stir Spot Welding and its Performance", *J. Mater. Process. Technol.*, vol. 210, no. 6–7, pp. 844–851, Apr. 2010.

[63] D. Fairchild, A. Kumar, S. Ford, N. Nissley, R. Ayer, H. Jin, A. Ozekcin, "Research Concerning the Friction Stir Welding of Linepipe Steels", *Trends in Welding Research, Proceedings of the 8th International Conference*, pp. 371–380, 2009.

[64] Abaqus® 6.13-1 Documentation.

[65] F. Al-Badour, "Numerical and Experimental Investigation of Friction Stir Welding of Tube-Tubesheet Joints", *Ph. D. Dissertation*, King Fahd University of Petroleum & Minerals, Saudi Arabia, 2012.

[66] M. Buyuk, S. Kan, M. J. Loikkanen, "Explicit Finite Element Analysis of 2024-T3-T351 Aluminum Material Under Impact Loading for Airplane Engine Containment and Fragment Shielding", no. July, pp. 287–295, 2009.

[67] J. Davis, "Copper and Copper Alloys", *ASM international*, 2001.

[68] G. R. Johnson and W. H. Cook, "A Constitutive Model and Data for Metals Subjected to Large Strains, High Strain Rates and High Temperatures", *Proceedings of the 7th International Symposium on Ballistics*, vol. 21, pp. 541–547, 1983.

[69] http://www.convert-me.com/en/convert/density/denscopp.html., accessed 3/5/2015.

[70] L. Z. Jin and R. Sandström, "Numerical Simulation of Residual Stresses for Friction Stir Welds in Copper Canisters", *J. Manuf. Process.*, vol. 14, no. 1, pp. 71–81, 2012.

[71] H. Schmidt and J. Hattel, "A Local Model for the Thermomechanical Conditions in Friction Stir Welding", *Model. Simul. Mater. Sci. Eng.*, vol. 13, no. 1, pp. 77–93, Jan. 2005.

[72] H. Wang, P. a. Colegrove, and J. F. dos Santos, "Numerical investigation of the tool contact condition during friction stir welding of aerospace aluminium alloy", *Comput. Mater. Sci.*, vol. 71, pp. 101–108, Apr. 2013.

[73] Alro Steel Tool & Die Steel Handbook E9-13.

Vitae

Name	: Ahmed Kamal Mahgoub Ali
Nationality	: Sudanese
Date of Birth	: 2/20/1990
Email	: ahmoda007@gmail.com
Address	: Almamora 84-33 Khartoum – Sudan
Academic Background	: BSC Mechanical Engineering Department, University of Khartoum – Sudan

Publications

1. Ahmed K. Mahgoub, A. Bazoune, F. A. A. Al-Badour, A. Shuaib, and G. M. Karrar, "Experimental Study and Numerical Modeling of Friction Stir Spot Welding of Pure Copper Lap Joint", in ASME 2014 International Mechanical Engineering Congress and Exposition, Montreal, Canada, Nov. 2014.

2. G. M. Karrar, A. N. Shuaib, F. A. Al-Badour, N. Merah and Ahmed Mahgoub "Friction stir welding of commercially pure copper", in ASME 2014 International Mechanical Engineering Congress and Exposition, Montreal, Canada, Nov. 2014.

3. Ahmed K. Mahgoub, F. Al-Badour, A. Bazoune, A. Shuaib and N. Merah "On-line Condition Monitoring of Friction Stir Spot Welding Tool using Vibration Measurements", ASME IMECE 2015 conference – US –Houston, (Accepted Abstract).